Numerical evaluation of a set of analytical infiltration equations.

L. Lassabatere, Rafaël Angulo-Jaramillo, J. Soria Ulgade, J. Simunek, R. Haverkamp

Numerical evaluation of a set of analytical infiltration equations

L. Lassabatere,[1] R. Angulo-Jaramillo,[2,3] J. M. Soria-Ugalde,[4] J. Šimůnek,[5] and R. Haverkamp[3]

Received 4 March 2009; revised 19 June 2009; accepted 19 August 2009; published 19 December 2009.

[1] In this paper, a set of analytical infiltration equations that are commonly used to evaluate one- and three-dimensional water infiltration from a surface disc source is studied. Both the quasi-exact analytical formulation and the related approximations for short and long times are assessed. The analytical properties of the quasi-exact formulation are evaluated using a proposed scaling procedure in order to define the validity domains of related approximations. Both quasi-exact and approximate analytical equations are then studied with respect to their ability to reproduce numerically generated cumulative infiltrations from a 10 cm radius disc source for four soils (sand, loam, silt, and silty clay) at several initial saturations. The quasi-exact formulation is suitable for sand, loam, and silt when their soil-dependent and saturation-independent shape parameters, γ and β, are properly chosen (between 0.75 and 1 and 0.3 and 1.7, respectively). Approximations derived for the same shape parameters can also be used, provided that their use is restricted to proposed validity intervals. However, none of these equations applies for silty clay, since its hydraulic properties do not fulfill the conditions required for the use of the quasi-exact formulation.

Citation: Lassabatere, L., R. Angulo-Jaramillo, J. M. Soria-Ugalde, J. Šimůnek, and R. Haverkamp (2009), Numerical evaluation of a set of analytical infiltration equations, *Water Resour. Res.*, *45*, W12415, doi:10.1029/2009WR007941.

1. Introduction

[2] Modeling water fluxes in the vadose zone linking surface waters with groundwater is important for understanding the hydrological cycle and the transfer of water-transported contaminants. Such modeling is usually based on the Richards' equation describing variably saturated water flow, unless preferential flow is involved [e.g., *Feddes et al.*, 1988]. In any case, such modeling requires knowledge of soil hydraulic properties, such as the water retention curve $h(\theta)$ and the hydraulic conductivity function $K(\theta)$.

[3] Analysis of water infiltration experimental data has become a widely used practice for obtaining soil hydraulic properties [e.g., *Perroux and White*, 1988; *Jacques et al.*, 2002]. Several experimental devices, often based on the tension disc infiltrometer or in situ lysimeters, have been developed for this purpose. Collected infiltration data are then inversely analyzed using either analytical or numerical models [e.g., *Šimůnek and van Genuchten*, 1996; *Mallants et al.*, 1997; *Šimůnek et al.*, 1998; *Angulo-Jaramillo et al.*, 2000]. Among many water infiltration experiments, the Beerkan method, consisting of water infiltrating from a single infiltration ring at a zero pressure head [*Braud et al.*, 2005], proved to be a low cost and robust method for characterizing soil hydraulic properties, even at the watershed scale [*Haverkamp et al.*, 1996; *Galle et al.*, 2001; *Braud et al.*, 2003]. *Lassabatere et al.* [2006] proposed the "BEST" (Beerkan Estimation of Soil Transfer parameters) algorithm for estimating the entire set of unsaturated soil hydraulic properties using the inverse analysis of particle size distribution and the water cumulative infiltration curve obtained by the Beerkan method.

[4] Independent of the water infiltration device, there is great need for an accurate description of one- (1-D) and three-dimensional (3-D) water infiltration from a surface disc source. Several analytical solutions have been proposed to provide either approximate [*Braester*, 1973; *Salvucci and Entekhabi*, 1994] or exact [*Green and Ampt*, 1911; *Parlange et al.*, 1985; *Basha*, 1999, 2002; *Zhu and Mohanty*, 2002] solutions for 1-D water infiltration. However, most of these solutions are based on simplifying assumptions related to soil hydraulic properties, such as constant soil water diffusivity, or use inappropriate boundary conditions, such as a constant infiltration flux. Based on the analytical model for 1-D ponded cumulative infiltration [*Parlange et al.*, 1985; *Haverkamp et al.*, 1990], and its extension to three dimensions for a surface disc source [*Smetten et al.*, 1994], *Haverkamp et al.* [1994] proposed a set of analytical equations that were adapted for a constant water pressure head at the soil surface (h_{surf}) and a uniform initial water pressure head profile $h_0(z) = h_0$. Such a model proved to be consistent with infiltration data [*Clausnitzer et al.*, 1998]. A specific set was derived specifically for the Beerkan exper-

[1]Division Eau et Environnement, LCPC, Bouguenais, France.
[2]Laboratoire des Sciences de l'Environnement, Ecole Nationale des Travaux Publics de l'Etat, Vaulx-en-Velin, France.
[3]Laboratoire d'Étude des Transferts en Hydrologie et Environnement, CNRS, Grenoble, France.
[4]Departamento de Ingeniería Geomática e Hidráulica, Universidad de Guanajuato, Guanajuato, Mexico.
[5]Department of Environmental Sciences, University of California, Riverside, California, USA.

0043-1397/09/2009WR007941

iment, i.e., for $h_{surf} = 0$ and $\theta_{surf} = \theta_s$, but can be generalized for all other pressure heads, either negative or positive [*Ross et al.*, 1996].

[5] The 3-D cumulative infiltration, $I_{3D}(t)$, is related to the 1-D cumulative infiltration, $I_{1D}(t)$, by an additional term linear with time [*Smetten et al.*, 1994], usually written using equation (4) of *Haverkamp et al.* [1994]:

$$I_{3D}(t) = I_{1D}(t) + \frac{\gamma S^2}{r_d \Delta\theta}\, t \tag{1}$$

where $\Delta\theta$ ($= \theta_s - \theta_0$) stands for the difference between the saturated water content, θ_s, and the initial water content, θ_0, t is time, r_d is the radius of the disc source, γ is a shape parameter, and S stands for the sorptivity. The shape parameter γ is defined using the ratio between two estimators of the sorptivity [*Haverkamp et al.*, 1994], S and $\hat{S}$, the first of which is more precise [*Parlange*, 1975]:

$$\gamma = \sqrt{0.3}\,\frac{\hat{S}^2}{S^2} \tag{2a}$$

$$S^2 = 2\int_{\theta_0}^{\theta s} \frac{(\theta - \theta_o)}{f(\theta)}\, D(\theta)\, d\theta \tag{2b}$$

$$\hat{S}^2 = 2\,(\theta_s - \theta_o)\int_{\theta_0}^{\theta s} D(\theta)\, d\theta \tag{2c}$$

where D stands for the soil diffusivity, which is defined using the water retention curve $h(\theta)$ and the hydraulic conductivity function $K(\theta)$ as follows:

$$D(\theta) = K(\theta)\frac{dh}{d\theta} \tag{2d}$$

f in (2) stands for the flux concentration function [*Philip*, 1973], which can be precisely estimated using [*Parlange*, 1975]:

$$f(\theta) = \frac{2(\theta - \theta_0)}{\theta_s + \theta - 2\,\theta_0} \tag{2e}$$

[6] The 1-D cumulative infiltration equation can be derived using the analytical method for solving the 1-D Richards equation described by *Haverkamp et al.* [1990]. This leads to a quasi-exact implicit formulation for the 1-D cumulative infiltration [*Haverkamp et al.*, 1994, equation (5)]:

$$\frac{2\,\Delta K^2}{S^2}t = \frac{1}{1-\beta}\left[\frac{2\,\Delta K}{S^2}(I_{1D}(t) - K_0 t) - \ln\left(\frac{\exp\left(2\beta\frac{\Delta K}{S^2}(I_{1D}(t) - K_0 t)\right) + \beta - 1}{\beta}\right)\right] \tag{3}$$

where ΔK ($= K_s - K_0$) stands for the difference between hydraulic conductivities at the soil surface, K_s, and at initial saturations, K_0 [$= K(\theta_0)$], and where β is defined as an "integral" shape parameter [*Haverkamp et al.*, 1994]. The analytical method is based on the hypothesis that functions $K(\theta)$ and $D(\theta)$ are linked with the shape parameter β as follows:

$$\frac{K(\theta) - K_0}{K_s - K_0} = f(\theta)\left(1 - \beta\frac{\int_{\theta}^{\theta s}\frac{(\theta - \theta_0)D(\theta)}{f(\theta)}d\theta}{\int_{\theta_0}^{\theta s}\frac{(\theta - \theta_0)\,D(\theta)}{f(\theta)}d\theta}\right) \tag{4}$$

for all water contents $\theta \in [\theta_0, \theta_1]$.

[7] To simplify the solution, *Haverkamp et al.* [1994] derived the following direct time expansions, which can be regarded as good approximations for very short times, short times, and long times, respectively:

$$I_{1D}^{O(1)}(t) = S\sqrt{t} \tag{5a}$$

$$I_{1D}^{O(2)}(t) = S\sqrt{t} + \left(\frac{(2-\beta)}{3}\,\Delta K + K_0\right)t \tag{5b}$$

$$I_{1D}^{+\infty}(t) = K_s\, t + \frac{1}{2(1-\beta)}\,\ln\left(\frac{1}{\beta}\right)\frac{S^2}{\Delta K} \tag{5c}$$

Time derivatives of the quasi-exact formulation and of its approximations provide corresponding models for infiltration rates.

[8] The use of this set of analytical formulations requires adequate values for the shape parameters γ and β. While in their earlier work, *Haverkamp et al.* [1994] proposed an averaged value of 0.75 for γ and 0.6 for β, in their later studies [*Haverkamp et al.*, 1999, 2005] they considered the shape parameters as dependent on both the soil type and the initial water content. On the basis of equations (2a) and (4), *Fuentes et al.* [1992] proposed a direct formulation for the shape parameters as a function of the initial water content, θ_0, and hydraulic functions $K(\theta)$ and $D(\theta)$:

$$\beta(\theta_0) = 2 - 2\frac{\int_{\theta_0}^{\theta s}\frac{K(\theta) - K(\theta_0)}{K_s - K(\theta_0)}\,\frac{\theta_s - \theta_0}{\theta - \theta_0}D(\theta)\,d\theta}{\int_{\theta_0}^{\theta s} D(\theta)\,d\theta} \tag{6a}$$

$$\gamma(\theta_0) = \sqrt{0.3}\,\frac{2(\theta_s - \theta_0)\int_{\theta_0}^{\theta_s} D(\theta)\,d\theta}{\int_{\theta_0}^{\theta_s}(\theta_s + \theta - 2\theta_0)D(\theta)\,d\theta} \tag{6b}$$

[9] The use of the approximate equations requires knowledge of their validity domains. Since no study has yet focused on the proper definition of these time intervals, there is a risk that these equations may be used for times for which they are no longer valid.

[10] The objective of this paper is thus to study this set of equations, including both the quasi-exact formulation (equations (1) and (3)) and the related approximations (equation (5)) with respect to the optimal choice of the shape parameters β and γ, and their dependence on the soil type and initial water content conditions, and the definition of appropriate validity domains for the related approximations.

[11] First, we will define the scaled (dimensionless) one-dimensional cumulative infiltration, $I^*(t^*)$, and the scaled difference between three- and one-dimensional (3-D–1-D) cumulative infiltrations, $\Delta I^*(t^*)$. We will then show that $\Delta I^*(t^*)$ is a linear function of the scaled time t^*, using the shape parameter γ as the proportionality constant. We will also show that $I^*(t^*)$ depends only on the shape parameter β. We will evaluate $I^*(t^*)$ with respect to its approximate formulations and their validity domains as a function of the shape parameters. The scaling procedure will allow us to transform these dimensionless intervals into real time intervals for both 1-D and 3-D cumulative infiltrations. A similar approach will be used for infiltration rates.

[12] In the second step, the quasi-exact formulation and its approximations will be tested against numerically generated 1-D and 3-D cumulative infiltration data. The 3-D case will be for infiltration from a 10 cm radius disc source for four different soil types (sand, loam, silt, and silty clay) and several initial saturation conditions. Appropriate values for the shape parameters β and γ, and their dependence on the soil type and initial water content conditions, will then be estimated by fitting previously scaled numerical data to scaled functions $I^*(t^*)$ and $\Delta I^*(t^*)$. The fitted shape parameters will then be used in dimensional equations (1) and (3) and the adequacy of this analytical model will be discussed for each soil type and each initial saturation. Finally, the validity domains of the approximations will be determined as a function of the shape parameters for each soil type and initial saturation conditions, and the accuracy of both scaled and dimensional approximations will be discussed.

2. Theory: Analytical Analysis

2.1. Scaling Procedure and Scaled Variables $I^*(t^*)$ and $\Delta I^*(t^*)$

[13] The 3-D and 1-D cumulative infiltration equations (equations (1) and (3)) can be modified to result in simpler equations using the following procedure:

$$t^* = \frac{1}{1-\beta}\left[I^* - \ln\left(\frac{\exp(\beta I^*) + \beta - 1}{\beta}\right)\right] \tag{7a}$$

$$\Delta I^* = \gamma t^* \tag{7b}$$

where 1-D and 3-D cumulative infiltrations are related to the scaled 1-D cumulative infiltration, $I^*(t^*)$, and the scaled difference between 3-D and 1-D cumulative infiltrations, $\Delta I^*(t^*)$, through

$$t = \frac{S^2}{2\,\Delta K^2} t^* \tag{7c}$$

$$I_{1D} = \frac{S^2}{2\,\Delta K} I^* + K_0\, t \tag{7d}$$

$$I_{3D} = I_{1D} + \frac{S^4}{2\,\Delta K^2\, r_d\, \Delta\theta}\Delta I^* \tag{7e}$$

These formulations define the scaling factors related to time (γ_t), 1-D cumulative infiltration (γ_I), and the difference between 3-D and 1-D cumulative infiltrations ($\gamma_{\Delta I}$), as previously proposed [*Parlange et al.*, 1982; *Rasoulzadeh and Sepaskhah*, 2003; *Haverkamp et al.*, 2005; *Varado et al.*, 2006].

[14] Notice that the scaled difference $\Delta I^*(t^*)$ is proportional to the scaled time t^*, and that the shape parameter γ serves as the proportionality coefficient. The scaled 1-D cumulative infiltration $I^*(t^*)$ depends only on the shape parameter β. Approximations of (7a) and their validity domains, as well as its derivative with time t^*, i.e., the scaled infiltration rate, $q^*(t^*)$, can therefore be studied only with respect to β. Notice also that when the shape parameter β is close to zero, equation (7a) leads to the Green and Ampt model [*Green and Ampt*, 1911] (see Appendix A):

$$t^* = I^* - \ln(1 + I^*) \tag{8}$$

2.2. Analysis of $I^*(t^*)$ and Related Approximations

[15] Since for long times, $I^*(t^*)$ tends to infinity, the right term of equation (7a) can be simplified using the asymptotic behavior of exponential and logarithmic functions, leading to (see Appendix A):

$$I_{+\infty}{}^*(t^*) = t^* + \frac{1}{(1-\beta)}\ln\left(\frac{1}{\beta}\right) \tag{9}$$

[16] At very short times, $I^*(t^*)$ can be developed using a square-root-of-time series [*Philip*, 1969]. Implementation of such serial expansion into equation (7a) leads to the following definitions for the first- and second-order approximations:

$$I^*_{O(1)}(t^*) = \sqrt{2t^*} \tag{10a}$$

$$I^*_{O(2)}(t^*) = \sqrt{2t^*} + \frac{2-\beta}{3}\, t^* \tag{10b}$$

[17] Validity domains of these approximations are directly linked to their accuracy, and thus to corresponding relative errors:

$$\xi^*_{Io(1)}(t^*) = \frac{\left|I^*(t^*) - I^*_{O(1)}(t^*)\right|}{I^*(t^*)} \tag{11a}$$

$$\xi^*_{Io(2)}(t^*) = \frac{\left|I^*(t^*) - I^*_{O(2)}(t^*)\right|}{I^*(t^*)} \tag{11b}$$

$$\xi^*_{I+\infty}(t^*) = \frac{\left|I^*(t^*) - I^*_{+\infty}(t^*)\right|}{I^*(t^*)} \tag{11c}$$

Table 1. Analytical Expressions and Approximations for Scaled and 3-D Dimensional Cumulative Infiltration and Infiltration Rate

	Scaled Cumulative Infiltration		Scaled Infiltration Rate	
	$I^*(t^*, \beta)$	Time Restriction	$q^*(t^*, \beta)$	Time Restriction
All times	$t^* = \frac{1}{1-\beta}\left[I^* - \ln\left(\frac{\exp(\beta I^*)+\beta-1}{\beta}\right)\right]$	None	$1 + \frac{\beta}{\exp(\beta I^*)-1}$	None
Very short times	$\sqrt{2\,t^*}$	$\le t^*_{Io(1)}\ t(\xi^*, \beta)$[a]	$\frac{1}{\sqrt{2\,t^*}}$	$\le t^*_{qo(1)}(\xi^*, \beta)$[a]
Short times	$\sqrt{2\,t^*} + \frac{2-\beta}{3}\,t^*$	$\le t^*_{Io(2)}(\xi^*, \beta)$[a]	$\frac{1}{\sqrt{2\,t^*}} + \frac{2-\beta}{3}$	$\le t^*_{qo(2)}(\xi^*, \beta)$[a]
Long times	$t^* + \frac{1}{1-\beta}\ln\left(\frac{1}{\beta}\right)$	$\ge t^*_{I+\infty}(\xi^*, \beta)$[a]	1	$\ge t^*_{+\infty}(\xi^*, \beta)$[b]
	Dimensional Cumulative Infiltration		**Dimensional Infiltration Rate**	
	$I_{3D}(t)$	Time Restriction	$q_{3D}(t)$	Time Restriction
All times	$\frac{S^2}{2\,\Delta K}\,I^* + \left(K_0 + \frac{\gamma S^2}{r_d\,\Delta\theta}\right)t$	None	$\Delta K\,q^* + K_0 + \gamma\,\frac{S^2}{r_d\,\Delta\theta}$	None
Very short times	$S\,\sqrt{t}$	$\le \frac{S^2}{2\,\Delta K^2} t^*_{Io(1)}(\xi^*, \beta)$	$S\,\sqrt{t}$	$\le \frac{S^2}{2\,\Delta K^2}\,t^*_{qo(1)}(\xi^*, \beta)$
Short times	$S\,\sqrt{t} + \left(\frac{(2-\beta)}{3}\,\Delta K + K_0 + \frac{\gamma S^2}{r_d\Delta\theta}\right)\,t$	$\le \frac{S^2}{2\,\Delta K^2} t^*_{Io(2)}(\xi^*, \beta)$	$\frac{S}{\sqrt{2t}} + \left(\frac{(2-\beta)}{3}\,\Delta K + K_0 + \frac{\gamma S^2}{r_d\Delta\theta}\right)$	$\le \frac{S^2}{2\,\Delta K^2}\,t^*_{qo(2)}(\xi^*, \beta)$
Long times	$\left(K_s + \frac{\gamma S^2}{r_d\Delta\theta}\right)\,t + \frac{1}{2\,(1-\beta)}\ln\left(\frac{1}{\beta}\right)\,\frac{S^2}{\Delta K}$	$\ge \frac{S^2}{2\,\Delta K^2} t^*_{I+\infty}(\xi^*, \beta)$	$\left(K_s + \frac{\gamma S^2}{r_d\Delta\theta}\right)$	$\ge \frac{S^2}{2\,\Delta K^2}\,t^*_{q+\infty}(\xi^*, \beta)$

[a]Calculated numerically from the study of the error functions.
[b]Calculated numerically from the study of the error functions or estimated through equation (13).

Since it can be shown numerically that the function $\xi^*_{I+\infty}(t^*)$ is monotonously decreasing in the interval $\Re^{*+}$, defining a bijection from $\Re^*+$ to (0,1), the inverse function $t^*_{I+\infty}(\xi^*)$ can also be defined. Therefore, for any time $t^* \ge t^*_{I+\infty}(\xi^*)$, the relative error $\xi^*(t^*)$ will be smaller than the given tolerance ξ^*. The validity domain for $I^*_{+\infty}(t^*)$ is thus defined as the time interval $[t^*_{I+\infty}(\xi^*), +\infty)$. A similar approach demonstrates that validity domains for $I^*_{O(1)}(t^*)$ and $I^*_{O(2)}(t^*)$ correspond to time intervals $[0, t^*_{Io(1)}(\xi^*)]$ and $[0, t^*_{Io(2)}(\xi^*)]$, respectively, where $t^*_{Io(1)}(\xi^*)$ and $t^*_{Io(2)}(\xi^*)$ are the inverse functions of $\xi^*_{Io(1)}(t^*)$ and $\xi^*_{Io(2)}(t^*)$, respectively. Dimensionless times $t^*_{I+\infty}(\xi^*)$, $t^*_{Io(1)}(\xi^*)$, and $t^*_{Io(2)}(\xi^*)$ are referred to as long-time, first-order and second-order approximation validity times. Since there are no analytical expression available for evaluating these validity times, they will be calculated numerically in the Results section.

2.3. Analysis of $q^*(t^*)$ and Related Approximations

[18] An actual scaled infiltration rate $q^*(t^*)$ can be obtained by evaluating the derivative of $I^*(t^*)$ (7a) with respect to time t^*, leading to (see Appendix B):

$$q^*(I^*) = 1 + \frac{\beta}{\exp(\beta I^*) - 1} \tag{12}$$

[19] When time t^* tends to infinity, $I^*(t^*)$ also tends to infinity, and thus $q^*(I^*)$ tends to unity, which defines the steady state approximation $q^*_{+\infty}(t^*)$. Given a tolerance ξ^*, the flow rate is lower than unity plus the tolerance ξ^*, provided time is larger than the steady state validity time $t^*_{q+\infty}(\xi^*)$ defined as (see Appendix B):

$$t^*_{q+\infty}(\xi^*) = \frac{1}{(1-\beta)}\ln\left(\frac{\left(1+\frac{\beta}{\xi^*}\right)^{\frac{1}{\beta}}}{1+\frac{1}{\xi^*}}\right) \tag{13}$$

The validity domain for the steady state expansion $q^*_{+\infty}(t^*)$ is then defined as $[t^*_{q+\infty}(\xi^*), +\infty)$.

[20] As time approaches zero, $I^*(t^*)$ tends to zero, and thus $q^*(t^*)$ approaches infinity (see (12)). Expanding equation (12) for small I^* leads to (see Appendix B):

$$q^*_{\delta(1)}(I^*) = \frac{1}{I^*} \tag{14a}$$

$$q^*_{\delta(2)}(I^*) = \frac{1}{I^*} + 1 - \frac{\beta}{2} \tag{14b}$$

These approximations can be combined with the short-time expansions of $I^*(t^*)$ to give the analytical expressions for the first- and second-order approximations for $q^*(t^*)$:

$$q^*_{\delta(1)}(t^*) = \frac{1}{\sqrt{2}}t^{*-\frac{1}{2}} \tag{15a}$$

$$q^*_{\delta(2)}(t^*) = \frac{1}{\sqrt{2}}t^{*-\frac{1}{2}} + \frac{2-\beta}{3} \tag{15b}$$

Note that the steady state and short-time approximations of $q^*(t^*)$ correspond to time derivatives of approximations of $I^*(t^*)$. Note also that, from a mathematical point of view, deriving the expressions for $q^*(t^*)$ using serial expansions, rather than taking directly the derivative of the serial functions for $I^*(t^*)$, is the proper approach (see Appendix B). It has been previously demonstrated that directly derivating term by term serial expansions can lead to inappropriate functions; the direct derivation of serial functions requires certain conditions.

[21] As was the case for cumulative infiltration, the validity domains for the first- and second-order approxima-

tions of infiltration rates can be evaluated from relative errors:

$$\xi^*_{qo(1)} = \frac{\left|q^*(t^*) - q^*_{\partial(1)}(t^*)\right|}{q^*(t^*)} \tag{16a}$$

$$\xi^*_{qo(2)} = \frac{\left|q^*(t^*) - q^*_{\partial(2)}(t^*)\right|}{q^*(t^*)} \tag{16b}$$

Like those for scaled cumulative infiltration, functions $\xi^*_{qo(1)}$ and $\xi^*_{qo(2)}$ are monotonously increasing (see the Result section). Therefore, the validity domains for approximations $q^*_{\partial(1)}$, $q^*_{\partial(2)}$ are defined as time intervals $(0,t^*_{qo(1)}(\xi^*)]$ and $(0,t^*_{qo(2)}(\xi^*)]$, where $t^*_{qo(1)}(\xi^*)$ and $t^*_{qo(2)}(\xi^*)$ are inverse functions of $\xi^*_{qo(1)}(t^*)$ and $\xi^*_{qo(2)}(t^*)$, respectively. The first- and second-order validity times, $t^*_{qo(1)}(\xi^*)$ and $t^*_{qo(2)}(\xi^*)$, respectively, can, again, be calculated numerically (see the Result section). The steady state validity time is defined exactly using equation (13).

[22] The scaled variables and their analytical properties, i. e., their related approximations and validity times, are given in Table 1. Since in this section, both the cumulative infiltration and the infiltration rate have been shown to be time and β dependent, they have to been referred to as $I^*(t^*, \beta)$ and $q^*(t^*, \beta)$. Similarly the scaled difference between 3-D and 1-D, $\Delta I^*(t^*, \gamma)$, has to be regarded as both time and γ dependent.

2.4. Derivation of Dimensional $I_{1D}(t)$, $I_{3D}(t)$, $q_{1D}(t)$, and $q_{3D}(t)$ and Their Validity Domains

[23] Dimensional 1-D and 3-D quasi-exact cumulative infiltrations can then be defined using the scaled cumulative infiltration, the scaled difference between 3-D and 1-D cumulative infiltrations, and the definition of scaling factors (γ_t, γ_I, and $\gamma_{\Delta I}$) using equation (7):

$$I_{1D}(t) = \frac{S^2}{2\,\Delta K} I^*\left(\frac{2\Delta K^2\, t}{S^2}, \beta\right) + K_0\, t \tag{17a}$$

$$I_{3D}(t) = \frac{S^2}{2\,\Delta K} I^*\left(\frac{2\,\Delta K^2\, t}{S^2}, \beta\right) + K_0\, t + \frac{S^4}{2\, r_d\, \Delta\theta\, \Delta K^2} \cdot \Delta I^*\left(\frac{2\,\Delta K^2\, t}{S^2}, \gamma\right) \tag{17b}$$

Infiltration rates can be derived as time derivatives of the above equations:

$$q_{1D}(t) = \Delta K\, q^*\left(\frac{2\Delta K^2\, t}{S^2}, \beta\right) + K_0 \tag{17c}$$

$$q_{3D}(t) = \Delta K\, q^*\left(\frac{2\Delta K^2\, t}{S^2}, \beta\right) + K_0 + \gamma \frac{S^2}{r_d\, \Delta\theta} \tag{17d}$$

Similarly, the dimensional approximations can be derived from equation (17) and the scaled approximations. Such derivation produces the same expressions as those developed by *Haverkamp et al.* [1994], i.e., equation (5).

[24] The discrepancy between the dimensional approximations and the dimensional quasi-exact formulation can be linked to the accuracy of the scaled functions. Let the relative errors be defined for scaled, $y^*_{approx}(t^*)$ and $y^*(t^*)$, and dimensional, $y_{approx}(t)$ and $y(t)$, variables as follows:

$$\xi_{approx}(t, y) = \frac{\left|y(t) - y_{approx}(t)\right|}{y(t)} \tag{18a}$$

$$\xi^*_{approx}(t^*, y^*) = \frac{\left|y^*(t) - y^*_{approx}(t)\right|}{y^*(t)} \tag{18b}$$

where y stands for either dimensional q or I, and y^* for scaled I^* or q^*, in both one dimension and three dimensions. The use of scaling equation (17) leads to the following relationships:

$$\xi_{approx}(t, I_{1D}) = \frac{1}{1 + \dfrac{K_0}{\Delta K}\dfrac{t^*}{I^*}}\, \xi^*_{approx}\,(t^*, I^*) \tag{19a}$$

$$\xi_{approx}(t, q_{1D}) = \frac{1}{1 + \dfrac{K_0}{\Delta K}\dfrac{1}{q^*}}\, \xi^*_{approx}\,(t^*, q^*) \tag{19b}$$

$$\xi_{approx}(t, I_{3D}) = \frac{1}{1 + \left(\dfrac{K_0}{\Delta K} + \dfrac{\gamma\, S^2}{r_d\, \Delta\theta}\right)\dfrac{t^*}{I^*}}\, \xi^*_{approx}\,(t^*, I^*) \tag{19c}$$

$$\xi_{approx}(t, q_{3D}) = \frac{1}{1 + \left(\dfrac{K_0}{\Delta K} + \dfrac{\gamma\, S^2}{r_d\, \Delta\theta}\right)\dfrac{1}{q^*}}\, \xi^*_{approx}\,(t^*, q^*) \tag{19d}$$

Insofar as $q^*(t^*)$ is between infinity and unity, $1/q^*$ and t^*/I^* are always between zero and unity, implying that:

$$\frac{1}{1 + \dfrac{K_0}{\Delta K}}\, \xi^*_{approx}\,(t^*, y^*) \le \xi_{approx}(t, y_{1D}) \le \xi^*_{approx}\,(t^*, y^*) \tag{20a}$$

$$\frac{1}{1 + \dfrac{K_0}{\Delta K} + \dfrac{\gamma\, S^2}{r_d\, \Delta\theta}}\, \xi^*_{approx}\,(t^*, y^*) \le \xi_{approx}(t, y_{3D}) \le \xi^*_{approx}\,(t^*, y^*) \tag{20b}$$

Equation (19) shows that relative errors for dimensional approximations are smaller than the errors for scaled approximations for both one dimension and three dimensions. Consequently, relative errors are smaller than the tolerance ξ in intervals with boundaries defined as the product of the time scaling factor and the scaled validity times.

Table 2. Values for Hydrodynamic Parameters for the Four Studied Soils

	Sand	Loam	Silt	Silty Clay
n	2.68	1.56	1.37	1.09
I	0.5	0.5	0.5	0.5
θ_r	0.045	0.078	0.034	0.07
θ_s	0.43	0.43	0.46	0.36
K_s (cm min^{-1})	4.95×10^{-1}	1.73×10^{-2}	4.17×10^{-3}	3.33×10^{-4}
h_g (cm)	6.90	27.8	62.5	200

[25] Such an approach leads to the following definition of the validity time for any dimensional approximation $y_{approx}(t)$, revealing its dependency on the initial saturation degree Se_0:

$$t^{xD}_{y\_approx}(Se_0,\beta) = \frac{S^2}{2\,\Delta K^2}\; t^{*}_{y\_approx}\,(\beta) \tag{21a}$$

$$t^{xD}_{y\_approx}(Se_0,\beta) = \frac{S^2(\theta(Se_0),\theta_s)}{2\,(K_s - K(\theta(Se_0)))^2}\; t^{*}_{y\_approx}\,(\beta) \tag{21b}$$

where x is equal to either 1 or 3 and $t^{*}_{y\_approx}(\beta)$ stands for the corresponding scaled validity time. When the parameter β varies little with the initial saturation degree, the scaled validity time, $t^{*}_{y\_approx}(\beta)$, remains constant. Dimensional times for nonzero initial saturation degrees $t^{xD}_{y\_approx}(Se,\ \beta)$ can then be calculated using the dimensional time for a zero initial saturation degree $t^{xD}_{y\_approx}(0,\ \beta)$ using:

$$t^{xD}_{y\_approx}(Se_0,\beta) = R(Se_0)\; t^{xD}_{y\_approx}(0,\beta) \tag{22a}$$

$$R(Se_0) = \frac{S^2(\theta(Se_0),\theta_s)}{S^2(\theta_r,\theta_s)}\,\frac{K_s^2}{(K_s - K(Se_0))^2} \tag{22b}$$

Reference validity times and ratios are discussed in the Results section. The analytical properties of the dimensional variables (approximations and validity times) are presented in Table 1.

3. Material and Methods: Numerical Modeling

[26] Beerkan infiltration experiments (for ponding conditions, i.e., $\theta_f = \theta_s$) were modeled for four soil types and for several uniform initial saturation conditions (i.e., h_0, θ_0), which correspond to conditions, for which equation (3) was developed [*Haverkamp et al.*, 1994]. Soil hydraulic parameters for four studied soil types, i.e., sand, loam, silt, and silty clay, were obtained from the ROSETTA database [*Schaap et al.*, 2001] implemented into HYDRUS codes [*Šimůnek and van Genuchten*, 2008; *Šimůnek et al.*, 2008]. Their water retention curves and hydraulic conductivity functions were described using the van Genuchten-Mualem model [*van Genuchten*, 1980; *Mualem*, 1976]:

$$\begin{cases} \theta(h) = \theta_r + (\theta_s - \theta_r)\left[1 + \left(\dfrac{|h|}{h_g}\right)^n\right]^{-m} & h < 0 \\ \theta(h) = \theta_s & h \geq 0 \end{cases} \tag{23a}$$

$$m = 1 - \frac{1}{n} \tag{23b}$$

$$K(h) = K_s \cdot K_r(h) = K_s \cdot S_e^l\left[1 - \left(1 - S_e^{1/m}\right)^m\right]^2 \tag{23c}$$

where θ_r and θ_s denote the residual and saturated water contents, respectively; K_r and K_s are the relative and saturated hydraulic conductivities, respectively, h_g is the scale parameter for water pressure, n is a pore size distribution index, and l is a pore connectivity parameter, assumed to be 0.5 by *Mualem* [1976]. Soil hydraulic parameters for four soil textural classes are given in Table 2.

[27] One dimensional water flow was modeled using HYDRUS-1D [*Šimůnek et al.*, 2008]. The transport domain was assumed to be 2 m deep for sand, 1 m for loam and silt, and 40 cm for silty clay. For the initial conditions, values of h_0 and θ_0 were chosen to represent saturations common for field conditions, as well as to explore the entire saturation range from dry soils to soils close to full saturation, i.e., from about 5% to 95% (Table 3). Free drainage (or unit hydraulic gradient) was selected as the lower boundary condition, which is often used to represent conditions with a deep water table. Finite elements (FE) of 2 mm were used to discretize the transport domain for all soils except silty loam, for which 0.2 mm elements were used for runs with low initial pressure heads ($5 \cdot 10^4$ and $2 \cdot 10^{10}$ cm). This spatial discretization was chosen using a sensitivity analysis. Several FE meshes were tested, and numerical

Table 3. Initial Conditions in Terms of Pressure Heads h_0 and Corresponding Saturation Degrees Se_0 Used in Numerical Simulations for Four Studied Soils

Sand		Loam		Silt		Silty Clay	
h_0 (cm)	Se_0 (%)	h_0 (cm)	Se_0 (%)	h_0 (cm)	Se_0 (%)	h_0 (cm)	Se_0 (%)
−5	80.2,	−20	84.5	−40	89.0	−40	98.7
−10	44.0	−40	69.4	−60	83.5	−60	98.1
−20	16.1	−60	59.1	−80	78.9	−80	97.4
−40	5.2	−80	51.9	−100	75.0	−100	96.9
−60	2.6	−100	46.6	−500	45.6	-10^3	85.4
−80	1.6	−300	26.2	-5×10^3	19.8	-5×10^4	60.8
−100	1.1	−500	19.7	-5×10^4	8.4	5×10^5	49.5
−1000	0.02	-10^3	13.4	-2×10^5	5.0	-5×10^6	40.2
		-5×10^3	5.5			-10^8	30.7
		-10^4	3.7			-2×10^{10}	19.1

results were plotted against mesh density. Maximum time was chosen to be higher than time needed to reach a steady state (a constant flow rate at the top). Minimum time steps were fixed at 10^{-3} min for sand, loam and silt, and 10^{-4} min for silty clay. Precision tolerances for pressure heads and water contents were fixed for all soils at HYDRUS default values of 1 cm and 0.001, respectively.

[28] Three-dimensional water flow was simulated using the axisymmetrical option of HYDRUS [*Šimůnek et al.*, 2006]. Transport domains were assumed to be 40 cm in both radial and vertical directions. Quadrilateral FE elements of 2 mm were used for all soils. The same initial conditions were used as in the 1-D analysis (Table 3). No flux boundary conditions were used at all boundaries except for the bottom of the transport domain where free drainage was used, and the center part (a radius of 10 cm) of the soil surface representing the infiltration disc where zero pressure head was applied. Parameters of the time discretization were the same as for 1-D numerical simulations.

[29] Simulation results included pressure head and water content maps, as well as dimensional cumulative infiltrations and infiltration rates. Other calculations and minimum least squares error optimizations were carried out using the scilab free code [*Campbell et al.*, 2006].

4. Results

[30] In what follows, we will first discuss the properties of the scaled quasi-exact functions $I^*(t^*, \beta)$ and $q^*(t^*, \beta)$ with respect to the shape parameter β and their approximations and associated validity domain. The scaled difference between 3-D and 1-D cumulative infiltrations will not be discussed any further because of its simplicity (a simple linear law). Second, the accuracy of analytical models will be evaluated by comparing them with numerically generated cumulative infiltrations for selected scenarios involving 3-D and 1-D water infiltrations into four soil types (sand, loam, silt, silty clay) and several initial saturation conditions. This comparison will allow us to discuss the shape parameters and validity domains of approximations.

4.1. Analytical Analysis of $I^*(t^*, \beta)$ and $q^*(t^*, \beta)$

4.1.1. Case of the Usual Value $\beta_0 = 0.6$

[31] Figure 1 shows scaled cumulative infiltration $I^*(t^*, \beta_0)$ and infiltration rate $q^*(t^*, \beta_0)$, as well as their long time/steady state, and first- and second-order approximations. All functions were evaluated for the shape parameter $\beta_0 = 0.6$. Related validity times are calculated assuming a tolerance ξ^*_0 of 2.5%. The scaled cumulative infiltration $I^*(t^*, \beta_0)$ and infiltration rate $q^*(t^*, \beta_0)$ curves have required properties, i.e., $I^*(t^*, \beta_0)$ increases with time t^* and is concave, and $q^*(t^*, \beta_0)$ decreases toward unity and is convex.

[32] The proposed analytical expressions (10) and (9) are good approximations of the scaled quasi-exact formulation (7a) for $I^*(t^*, \beta_0)$ in their validity intervals. Similarly, the proposed analytical expressions (15) are accurate approximation in their validity intervals for $q^*(t^*, \beta_0)$. This confirms the suitability of the proposed analytical expressions. As illustrated in Figures 1c–1d, the related relative errors $\xi^*_{I+\infty}(t^*, \beta_0)$ and $\xi^*_{q+\infty}(t^*, \beta_0)$ are monotonously decreasing and $\xi^*_{Io(1)}(t^*, \beta_0)$, $\xi^*_{Io(2)}(t^*, \beta_0)$, $\xi^*_{qo(1)}(t^*, \beta_0)$, and $\xi^*_{qo(2)}(t^*, \beta_0)$ are monotonously increasing functions. Consequently, the long-time approximation validity time $t^*_{I+\infty}(\xi^*, \beta_0)$ and the steady state validity time $t^*_{q+\infty}(\xi^*, \beta_0)$ are decreasing functions and the first- and second-order validity times $t^*_{Io(1)}(\xi^*, \beta_0)$, $t^*_{Io(2)}(\xi^*, \beta_0)$, $t^*_{qo(1)}(\xi^*, \beta_0)$, and $t^*_{qo(2)}(\xi^*, \beta_0)$ are increasing functions (Figures 1e–1f). For small tolerances ξ^*, the validity times increase in the following order: first order < second order < long time/steady state. For instance, for $\xi^* = \xi_0^* = 2.5\%$, these correspond to $0.006 < 0.74 < 2.73$ and $0.0015 < 0.26 < 4.13$ for $I^*(t^*, \beta_0)$ and $q^*(t^*, \beta_0)$, respectively. When the tolerance ξ^* increases, this order shifts to first order < long time/steady state < second order (Figure 1e–1f), and when $\xi^* > 0.15$ to long time < first order < second order. Intersections between the long time/steady state and second-order validity times correspond to a relative error of 5.5% and 12% for $I^*(t^*, \beta_0)$ and $q^*(t^*, \beta_0)$, respectively. This means that the quasi-exact formulations $I^*(t^*, \beta_0)$ and $q^*(t^*, \beta_0)$ can be replaced first with their second-order and then long-time/steady state approximations while having relative errors lower than 5.5% and 12%, respectively.

[33] It may be noted that relative errors are higher for $q^*(t^*, \beta_0)$ than for $I^*(t^*, \beta_0)$ (Figures 1c–1d). This means that the use of the approximation is less accurate for the infiltration rate than for the cumulative infiltration. Therefore, the validity domains for $q^*(t^*, \beta_0)$ need to be reduced for the first- and second-order approximations, and increased for the steady state approximation to ensure the same precision as for $I^*(t^*, \beta_0)$.

4.1.2. Sensitivity Analysis of $I^*(t^*, \beta)$ and $q^*(t^*, \beta)$ as a Function of β

[34] The scaled functions $I^*(t^*, \beta)$ and $q^*(t^*, \beta)$ were also studied with respect to the value of their shape parameter β. The value range of this parameter is not known a priori, even though it was originally restricted to between zero and unity for mathematical reasons related to the integration method developed by *Haverkamp et al.* [1990] and generalized by *Ross et al.* [1996]. In the latter study, the parameter β is regarded as an integral shape parameter, as suggested by *Haverkamp et al.* [1994], and thus allowed to have larger values. In agreement with its definition by (6a), (as suggested by *Fuentes et al.* [1992]) β is restricted here to values smaller than two (a positive value of the integrals 6a). The same constraint appears from the analysis of the first- and second-order approximations of $I^*(t^*, \beta)$. Since $I^*_{O(2)}(t^*, \beta)$ is defined as $I^*_{O(1)}(t^*, \beta)$ plus a second term involving β (see equation (10)), this term must be positive to ensure that $I^*_{O(1)}(t^*, \beta) \le I^*_{O(2)}(t^*, \beta) \le I^*(t^*, \beta)$. If such an inequality was not ensured, the second-order approximation would be less precise than the first-order approximation, which would be meaningless. Such a condition implies that:

$$\frac{2-\beta}{3} \ge 0, \text{i.e.}, \beta \le 2 \tag{24}$$

The scaled functions are therefore studied for $\beta \in [0,2]$. As explained above, the case with $\beta = 0$ corresponds to the Green and Ampt formulation.

[35] A change of the parameter β affects the scaled functions $I^*(t^*, \beta)$ and $q^*(t^*, \beta)$ without changing their monotonic behavior and analytical properties. In particular, relative errors of approximations keep the same monotonic properties with regard to time, and likewise similar

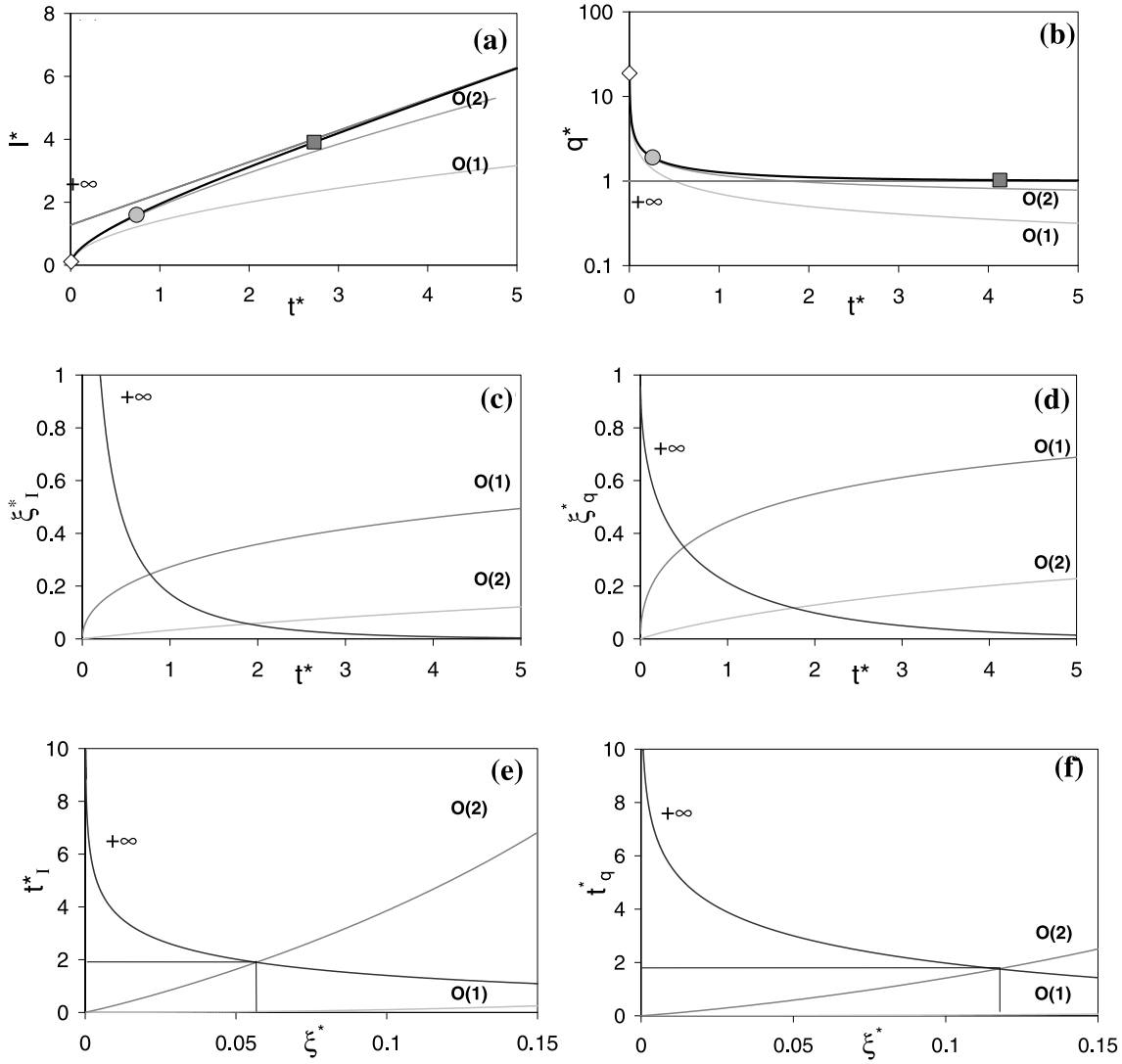

Figure 1. One-dimensional scaled analytical models for $\beta_0 = 0.6$. (a) Scaled cumulative infiltration $I^*(t^*, \beta_0)$ and (b) scaled infiltration rate $q^*(t^*, \beta_0)$ (black lines) along with related approximations (gray lines) and validity times (diamonds, very short time; gray circles, short time; gray squares, long time) calculated for the tolerance $\xi_0^* = 2.5\%$. Relative errors (ξ_I^* or ξ_q^*) of approximations as a function of time t^* for (c) scaled cumulative infiltration and (d) scaled infiltration rate. Validity times (t_I^* or t_q^*) as a function of the tolerance ξ^* (an inverse function) for (e) scaled cumulative infiltration and (f) scaled infiltration rate.

definitions of validity domains and validity times $t^*_{Io(1)}(\xi^*, \beta)$, $t^*_{Io(2)}(\xi^*, \beta)$, $t^*_{I+\infty}(\xi^*, \beta)$, $t^*_{qo(1)}(\xi^*, \beta)$, $t^*_{qo(2)}(\xi^*, \beta)$, and $t^*_{q+\infty}(\xi^*, \beta)$.

[36] Cumulative infiltrations $I^*(t^*, \beta)$ and infiltration rates $q^*(t^*, \beta)$ are decreasing functions with regard to β (Figures 2a and 2b). This decrease can be demonstrated for $I^*(t^*, \beta)$ by studying the right term of equation (7a) with regard to β. The effect of β on the validity times $t^*_{Io(1)}(\xi^*, \beta)$, $t^*_{Io(2)}(\xi^*, \beta)$, and $t^*_{I+\infty}(\xi^*, \beta)$ is illustrated in Figures 2c–2f. For the tolerance ξ^*_0, the time needed to apply the long-time approximation, $t^*_{I+\infty}(\xi^*_0, \beta)$, decreases with β (Figure 2c). This results from the fact that $q^*(t^*, \beta)$ decreases with β, i.e., a steady state is reached earlier when β increases (Figure 2b). The second-order approximation validity time, $t^*_{Io(2)}(\xi^*_0, \beta)$, roughly decreases with β (Figure 2c). The time interval that requires the application of the quasi-exact formulation $I^*(t^*, \beta)$ instead of its approximations, i.e., the time between the second-order and long-time approximations validity domains, reduces with β (Figure 2c). On the contrary, the first-order approximation validity time $t^*_{Io(1)}(\xi^*_0, \beta)$ is an increasing function until it reaches the value of the second-order validity time $t^*_{Io(2)}(\xi^*_0, \beta)$ for $\beta = 2$. This equality results from the fact that the first- and second-order approximations correspond when $\beta = 2$.

[37] Similar conclusions can be drawn for higher tolerances ξ^*. The value of ξ^* only affects the order between the validity times. For tolerances $\xi^*_0 = 2.5\%$ and $\xi^*_1 = 5\%$, the validity times are in the following order: $t^*_{Io(1)}(\xi^*_0, \beta) \leq t^*_{Io(2)}(\xi^*_0, \beta) \leq t^*_{I+\infty}(\xi^*_0, \beta)$ and $t^*_{Io(1)}(\xi^*_1, \beta) \leq t^*_{Io(2)}(\xi^*_1, \beta) \leq t^*_{I+\infty}(\xi^*_1, \beta)$ (Figures 2c and 2d). For a tolerance $\xi^*_2 = 7.5\%$

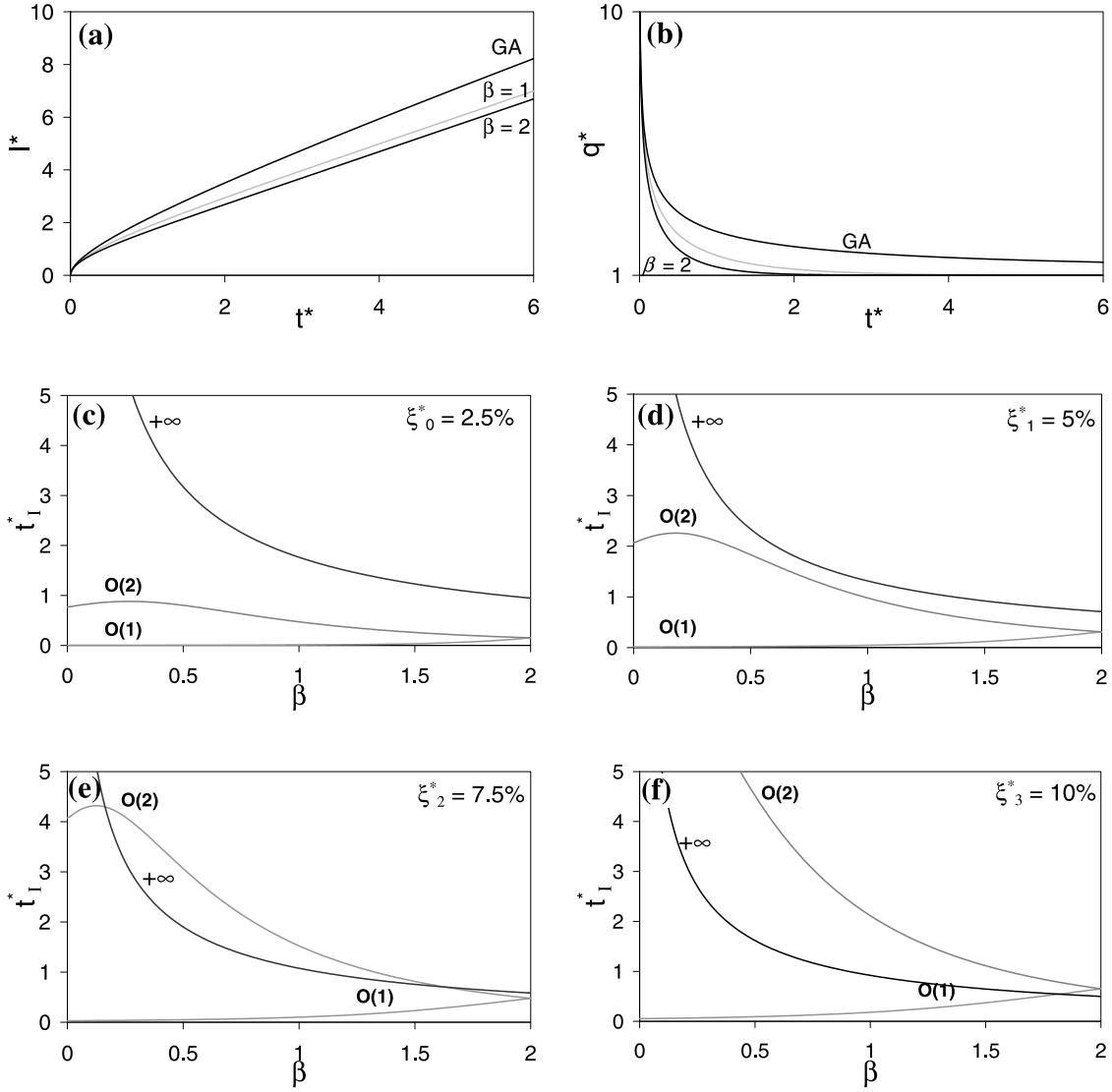

Figure 2. One-dimensional scaled analytical model as a function of β (from zero Green and Ampt (GA) model to two). (a) Scaled cumulative infiltrations $I^*(t^*, \beta)$, (b) infiltration rates q^* (t^*, β), and validity times for four tolerances: (c) $\xi_0^* = 2.5\%$, (d) $\xi_1^* = 5\%$, (e) $\xi_2^* = 7.5\%$, and (f) $\xi_3^* = 10\%$.

and values of β between 0.2 and 1.8, the order becomes: $t^*_{Io(1)}(\xi_2^*, \beta) \leq t^*_{I+\infty}(\xi_2^*, \beta) \leq t^*_{Io(2)}(\xi_2^*, \beta)$. The same order applies for a tolerance $\xi_3^* = 10\%$ and for any value of β (Figure 2f). This means that the second-order and long-time approximations can be successfully used to model infiltration for all values of β provided that a tolerance of 7.5% is acceptable for $I^*(t^*, \beta)$. Similar results are obtained for the validity times related to the scaled infiltration rates, except that in the latter cases, the related relative errors are higher.

4.2. Reproduction of Numerically Generated $I_{1D}(t)$, $I_{3D}(t)$, $q_{1D}(t)$ and $q_{3D}(t)$

4.2.1. Numerical Cumulative Infiltrations

[38] Numerical results are presented in terms of the dependence of 1-D and 3-D cumulative infiltrations upon initial saturations (Figures 3a–3d) and corresponding water content profiles for a specific initial saturation (Figure 3e–3h). For sand, both 1-D and 3-D cumulative infiltrations depend very little upon initial saturations, and are quasi linear (Figure 3a). Dimensionality mainly affects the slope, with an additional contribution of the 3-D lateral flux, due to capillary forces, to the 1-D vertical infiltration dominated by gravity. On the contrary, cumulative infiltrations are strongly saturation dependent for the other soils (Figures 3b–3d). The finer the soil, the more initial saturation dependent cumulative infiltrations. Moreover, as the soil becomes finer, the concavity of cumulative infiltrations becomes more pronounced, and the differences between 1-D and 3-D infiltrations become smaller. This means that water infiltration is less gravity and more capillarity driven. These numerical results are in complete agreement with experimental data [e.g., *Smith et al.*, 2002].

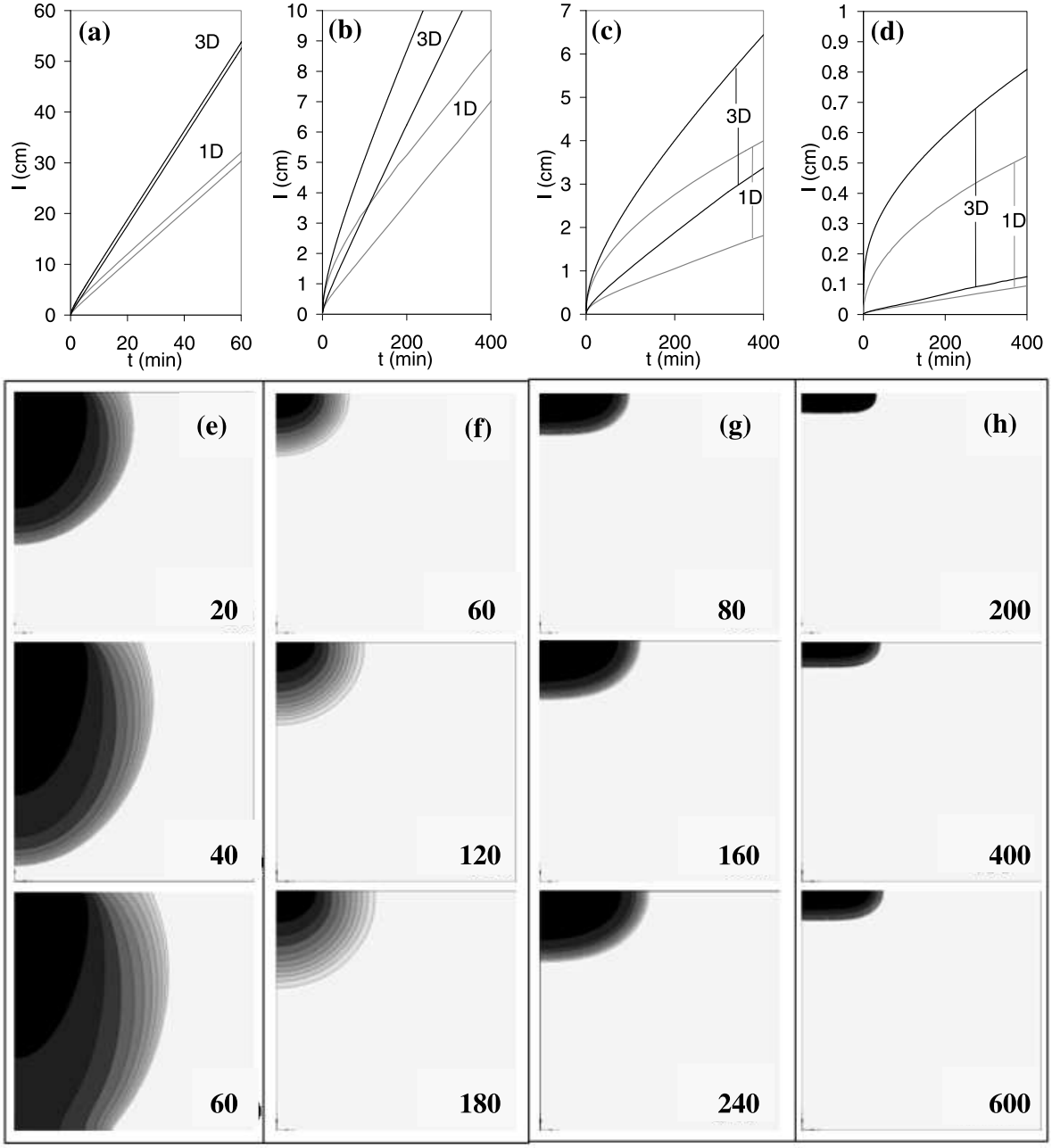

Figure 3. Numerically simulated data. Cumulative infiltrations (1-D and 3-D) as a function of the initial saturation Se_0 for a 10-cm radius disc source for (a) sand, (b) loam, (c) silt, and (d) silty loam (see Table 3 for Se_0 values). Water contents versus time (min) for (e) sand (h_0 = 40 cm, Se_0 = 10%), (f) loam (h_0 = 100 cm, Se_0 = 45%), (g) silt (h_0 = 500 cm, Se_0 = 45%), and (h) silty clay (h_0 = 5 10^4 cm, Se_0 = 50%); the isoclines corresponds to h_0 to zero by $h_0/10$ increments.

4.2.2. Modeling Scaled Data Using the Quasi-Exact Implicit Formulation

[39] In all cases, the correspondence between numerical and analytical models is evaluated using model relative errors defined as follows:

$$Er(x,y) = \frac{\hat{y}(x) - y(x)}{y(x)} \tag{25}$$

where $y(x)$ is the numerically generated value at point x and $\hat{y}(x)$ is the corresponding analytical model value. Note that positive values indicate model overestimations, whereas negative values indicate model underestimations.

[40] Scaled differences between 3-D and 1-D cumulative infiltrations $\Delta I^*_{num}(t^*)$ follow the same linear law for all initial saturations for loam and silt (Figure 4). A linear trend is also followed for sand, but the proportionality coefficient differs for the higher initial saturation Se_0 of 80%. The proportionality coefficient γ depends upon the soil type as detailed in Table 4. Optimized values of γ are close to the usual value of 0.75, as suggested by *Haverkamp et al.* [2005], for loam and silt, but substantially higher for

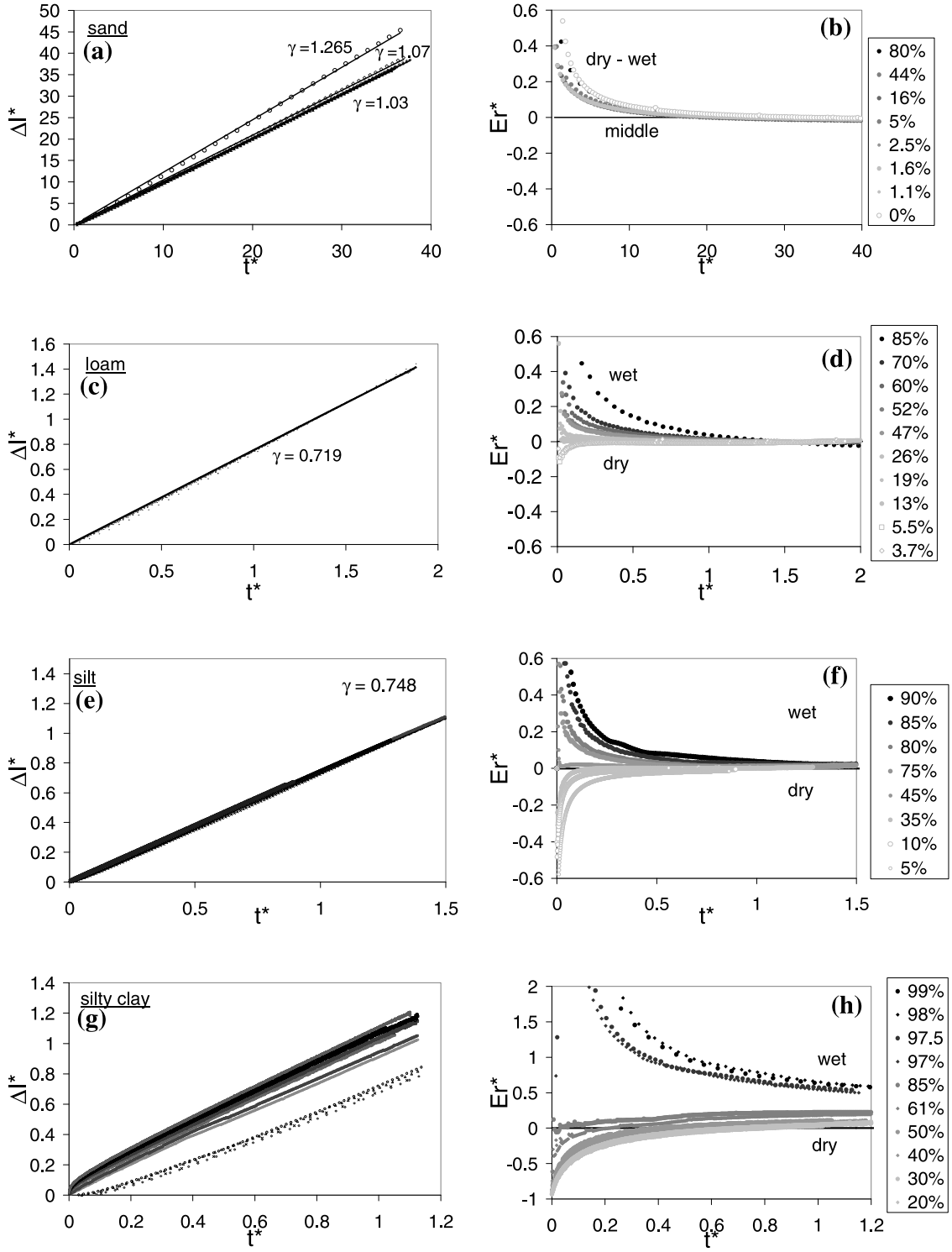

Figure 4. Scaled differences between 3-D and 1-D cumulative infiltrations $\Delta I^*_{num}(t^*)$ (numerically generated) and $\Delta I^*(t^*, \gamma)$ (obtained from quasi-exact formulations) as a function of (a, c, e, g) soil, initial saturation and parameter γ and (b, d, f, h) model errors. Initial saturations are shown on the right.

sand (1.03). Although all these values are significantly higher than those calculated using the relationship (6b) of *Fuentes et al.* [1992] (Table 4), they are in agreement with the previous work of *Warrick and Lazarovitch* [2007]. In particular, the latter authors also found lower values for medium textured soils (loam, silty loam) and larger values for coarser soils (sand) and finer soils (clay). Relative errors show that the linearity is well followed for large times t^*, but deviations from it may not be negligible close to zero (Figures 4b, 4d, and 4f), as previously highlighted by *Smetten et al.* [1994] and *Turner and Parlange* [1974]. In conclusion, the linear extension of 1-D cumulative infiltra-

Table 4. Proposed Values for the Shape Parameters β and γ Related to the Use of Quasi-Exact Formulation as a Function of the Soil Type[a]

	γ		β	
	Optimized	Fuentes	Optimized	Fuentes
Sand	1.03	0.587	0.334	0.535
Loam	0.756	0.593	1.25	1.22
Silt	0.748	0.59	1.56	1.46
Silty clay	0.977	0.575	1.65	1.90

[a]Quasi-exact formulations use equation (7). Also given are Fuentes values estimated [*Fuentes et al.*, 1992] using equations (6).

tion to 3-D using equation (7b) is accurate provided that the value of the shape parameter γ is chosen based on the soil type, and that the time is long enough.

[41] As with the scaled difference $\Delta I^*_{num}(t^*)$, the scaled cumulative infiltration $I^*_{num}(t^*)$ does not depend significantly on the initial saturation (Figure 5) and a unique value of β can be optimized independently of the initial saturation for sand, loam, and silt (Table 4). The resulting quasi-exact formulation for $I^*(t^*, \beta)$ is in good agreement with numerical data $I^*_{num}(t^*)$ (Figures 5a, 5c, and 5e). Model errors show a little autocorrelation (non random distribution of errors as a function of time), but are always lower than 10%, and usually below 5% (Figures 5b, 5d, and 5f). Although the model errors are slightly higher for silt, they stay in an acceptable range. It should be noted that for loam and silt, the model errors can be higher for very small times (Figures 5d and 5f). The optimized values of the shape parameter β vary significantly between different soil types, with a minimum value of 0.344 for sand and a maximum value of 1.56 for silt. These values differ significantly from the common value of 0.6 [*Haverkamp et al.*, 1994], but resemble values calculated using the *Fuentes et al.* [1992] relationship (6a). These results prove that the quasi-exact formulation (7a) is accurate for modeling the scaled cumulative infiltration, provided that the shape coefficient β reflects the soil type and is taken as proposed in Table 4.

[42] However, the textural class of silty clay remains an exception. Scaled numerically generated curves $I^*_{num}(t^*)$ do not fall on one line (Figure 5g), and model errors for several initial saturations are on the order of 10% and show a very strong autocorrelation (Figure 5h). The sign of the model errors indicates that numerically generated infiltration data are highly underestimated at low times t^* and overestimated at larger times t^*. Thus, the analytical model underestimates the concavity of numerically generated infiltration curves. Moreover, this discrepancy depends strongly upon the initial saturation (Figure 5h), indicating that an average value of β cannot be considered for all initial saturations. The linear law for the scaled 3-D−1-D difference is also no longer valid for silty clay (Figure 4g). Numerically generated differences $\Delta I^*_{num}(t^*)$ show a significant concavity that depends strongly on the initial saturation (Se_0). Relative errors are no longer acceptable for any considered times t^*(Figure 4h). This indicates that equation (7) is no longer valid for modeling scaled cumulative infiltrations in silty clay. This discrepancy results from the nonfulfillment of the constraints related to equation (4), which is documented in Figure 6 (a plot of relative errors between the right and left terms of equation (4) for the four soils). Note that these relative errors are significantly larger for silty clay than for the other three soils (Figure 6).

4.2.3. Modeling Dimensional Data Using the Quasi-Exact Formulation

[43] Dimensional modeled cumulative infiltrations are calculated using scaled cumulative infiltrations for optimized values of γ and β, and using scaling equation (17). This procedure is equivalent to the use of equations (1) and (3) along with optimized values of γ and β. Model errors are calculated using one- and three-dimensional numerically generated data and equation (25). Resulting model errors are in most cases lower than 10%, and quite frequently below 5% (Figures 7a−7f). Therefore, equations (3) and (1) are validated for such applications. Again, silty clay is an exception, with relative errors higher than 10% and even close to 50% in certain cases (Figure 7g−7h), resulting from the inadequacy of the scaled quasi-exact formulation as discussed above.

4.2.4. Modeling Scaled Data With Approximations and Related Validity Domains

[44] Approximate solutions are first studied with regard to scaled numerically generated data. The long-time and close-to-zero approximations are illustrated in Figures 8a, 8c, 8e, and 8g, together with scaled numerically generated data. The accuracy of approximations is evaluated using equation (25) and displayed in Figures 8b, 8d, 8f, and 8h. Maximum errors are then calculated in the validity intervals, determined for the tolerance $\xi^*_0 = 2.5\%$ and the optimized values of the shape parameter β.

[45] As with the quasi-exact formulation, the accuracy of approximate equations is not acceptable for silty clay (Figures 8g−8h). The model relative errors reach absolute values that are, in most cases, higher than 10−20%, which renders these approximations unsuitable to properly model water infiltration into silty clay. This was expected, as approximate equations were derived from the quasi-exact formulation, which was also not suitable for silty clay, as discussed above.

[46] The long-time and close-to-zero approximations seem accurate for sand, loam and silt (Figures 8a, 8c, and 8e) in their corresponding validity domains. The first-order approximation is characterized by a very sharp increase of model errors for all three soils (Figures 8b, 8d, and 8f). Very low values of the first-order validity time $t^*_{lo(1)}(\xi^*_0, \beta)$ for sand and loam, along with too few numerically generated data points in the related validity interval $[0, t^*_{lo(1)}(\xi^*_0, \beta)]$, did not allow for precise estimation of the model errors. For silt, the first-order approximation has a maximum model error close to 10% in the validity domain $[0, t^*_{lo(1)}(\xi^*_0, \beta)]$. For the second-order approximation, the model errors increase with time for sand (Figure 8b). For loam and silt, the model errors are quite high for very small times, especially for low initial saturations (Figures 8d and 8f). The errors then sharply decrease before reaching a minimum, and then begin increasing again (Figures 8d and 8f; arrows indicate the error minima). For these two soils, the error minima are located within the validity domains $[0, t^*_{lo(2)}(\xi^*_0, \beta)]$. Thus, after disregarding high errors close to zero (local phenomenon), the maximum error in absolute value is evaluated for the time interval $[t^*_{lo(2)}(\xi^*_0, \beta)/10, t^*_{lo(2)}(\xi^*_0, \beta)]$. In these intervals, the model relative

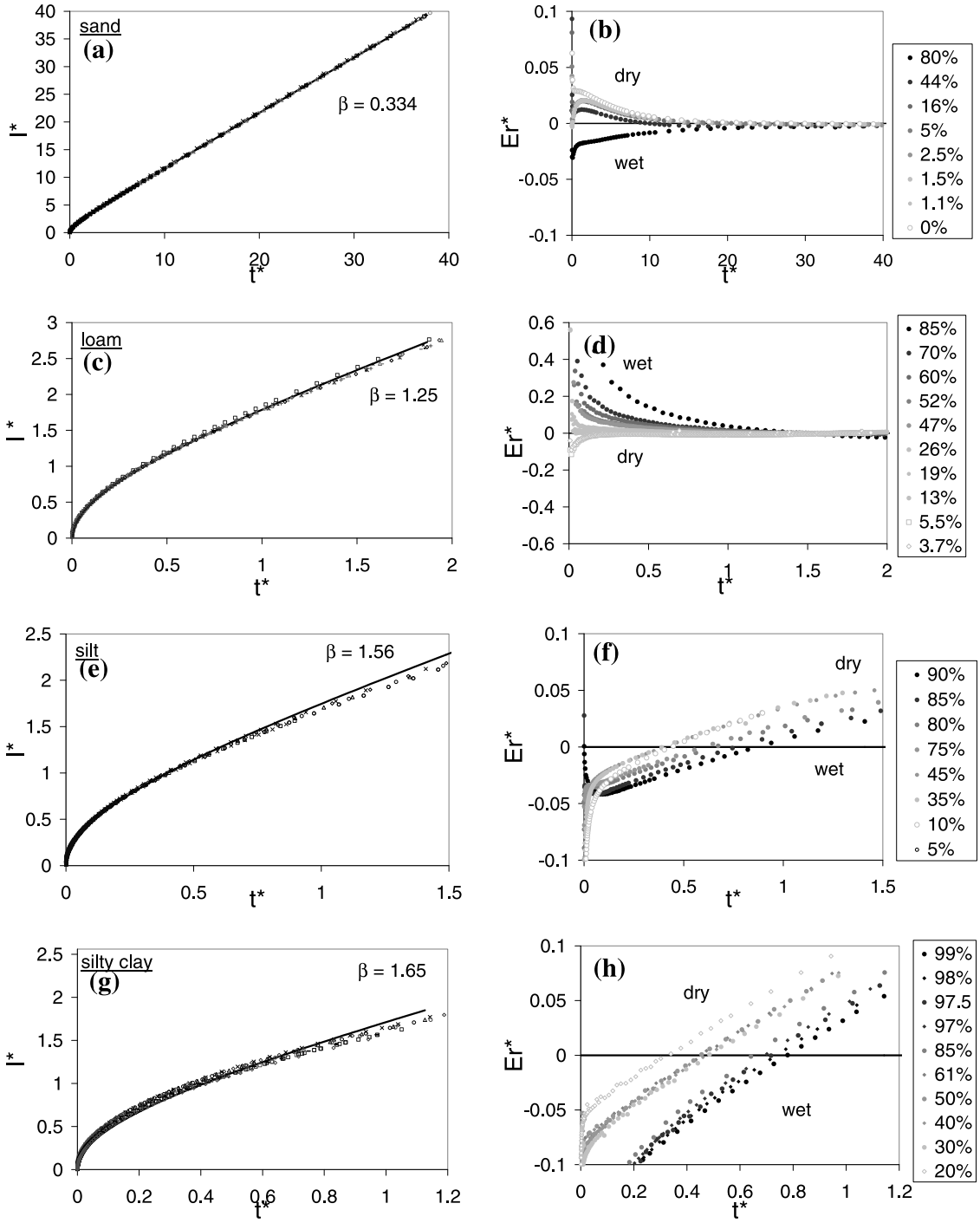

Figure 5. Scaled 1-D cumulative infiltrations $I^*_{num}(t^*)$, the quasi-exact formulations $I^*(t^*, \beta)$ and (a, c, e, g) estimated global values of β and (b, d, f, h) their model errors accuracy. Initial saturations are shown on the right.

errors are never higher than 5%. For the long-time approximations, the model errors are decreasing functions (Figures 8b, 8d, and 8f). When restricted to their validity intervals, $[t^*_{+\infty}(\xi^*), +\infty)$, the model errors are at most 5% for sand and loam, and a little higher for silt (between 5 and 7.5%). In conclusion, the approximations can be considered to be good estimations of numerically generated data in their corresponding validity domains.

4.2.5. Modeling Dimensional Data With Approximations and Related Validity Domains

[47] The relative error functions evaluating the accuracy of the dimensional approximate expansions in reproducing dimensional numerically generated data are similar to those shown in Figure 8 (data not shown). As with the scaled data, the maximum errors of dimensional expansions were determined for their validity domains, defined using scaled validity times and time scaling factors (equation (22)).

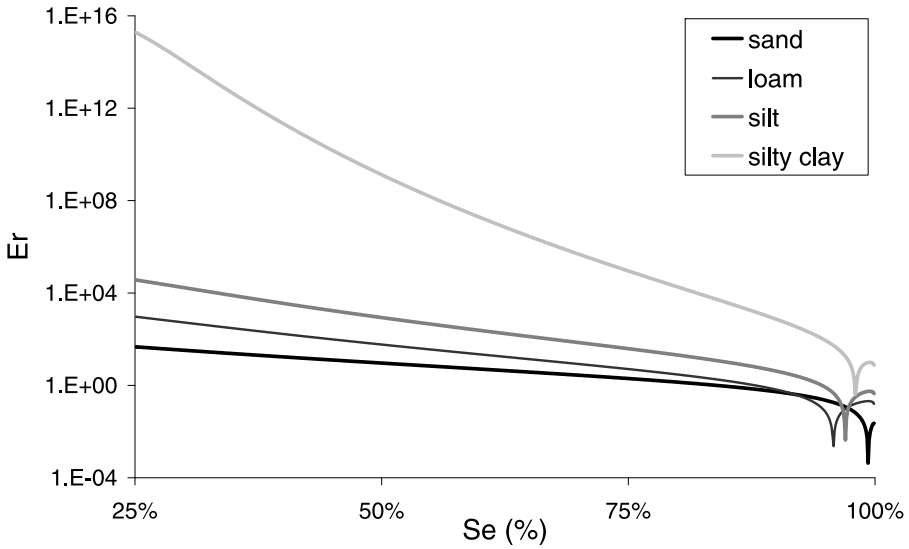

Figure 6. Relative error between the right and left terms of equation (4) for the four soils in function to the saturation degree during water infiltration between an initial saturation degree Se_0 = 25% and water saturation.

Again, to avoid high error values very close to zero time, the maximum errors were evaluated over the intervals $[t^{xD}_{I\_approx}(Se_0, \beta)/10, t^{xD}_{I\_approx}(Se_0, \beta)]$, as with the scaled data.

[48] The maximum errors for different soils and dimensions and zero initial saturation are given in Table 5. Errors for the first-order approximations for loam and sand could not be evaluated for the same reasons as with scaled data. Again, most errors were smaller than 5%, which indicates that the validity times were well chosen, and that the approximations were sufficiently accurate for their corresponding domains. As with the quasi-exact formulation, the approximations are no longer valid for silty clay, for which they produce errors higher than 20–25%. This indicates that the approximations, as with the quasi-exact solution, are not suitable for fine soils. The difficulty of applying common analytical models to describe infiltration into fine soils has been reported many times [e.g., *Lin and McInnes.*, 1995; *Messing and Jarvis*, 1993, *Vandervaere et al.*, 2000a, 2000b].

[49] The results discussed above indicate that the proposed validity intervals ensure an acceptable error of model predictions for sand, silt and loam. Values of the dimensional validity times are calculated using equation (22a) from the reference validity times $t_{Io(1)}(0, \beta)$, $t_{Io(2)}(0, \beta)$ and $t_{I+\infty}(0, \beta)$. Due to great differences in values of scaling factors for different soil types (sand < loam < silt < silty clay), corresponding reference times are of a different order of magnitude (Table 5 and Figure 9a). Their values provide practical information with respect to infiltration experiments, which usually have duration on the order of 1 to 2 h, and the cumulative infiltration is described at approximately one minute time intervals. For sands and loams, the validity times of the first-order approximations are too short to allow determination of sorptivity using the usual method [*Vandervaere et al.*, 2000a, 2000b]:

$$\lim_{t\to 0} \frac{dI_{1D}}{d\sqrt{t}} \approx \lim_{t\to 0} \frac{dI_{3D}}{d\sqrt{t}} \approx S \qquad (26)$$

The validity time for the second-order approximation, $t_{Io(2)}(0, \beta)$, is on the order of two minutes (Table 5). This suggests that, except for specific experimental protocols and setups (precise measurements of the infiltrated height and time), commonly collected information using the Beerkan protocol may require the use of the quasi-exact formulation or the long-time approximation (Figure 9a). For loam, the second-order approximation can be used only when short time steps are used in the experimental protocol. However, steady state conditions are reached only after about 3 h, which may be at the very end of infiltration experiments. For silt, the validity times for the first- and second-order approximations are on the order of few hours (Table 5), suggesting that the use of these approximations may be sufficient. On the contrary, steady state conditions are only reached after about 12 h, which is impractical for most experimental conditions, and thus the long-time approximations may not be used.

[50] When soils are initially wet, these restrictions may be relaxed, since dimensional times depend on the initial saturation (Figure 9b). In particular, it has been shown that values of β do not depend upon the initial saturation degree. Thus, as described in the theory section, the validity times are obtained by multiplying the reference validity time with the ratio R (equation (22)). These ratios can be reduced by several orders. Note that, independent of the soil type (except for sand close to saturation), there is a decreasing linear relation between the ratio R and the saturation degree Se_0 (Figure 9b). As a result, the validity times could be estimated using values given in Table 5 and assuming a simple decreasing linear relationship between R and the initial saturation (Se_0).

5. Conclusions

[51] Understanding and modeling the physical process of water infiltration into the soil are necessary for proper water management. The quasi-exact formulation and its related direct approximations developed by *Haverkamp et al.*

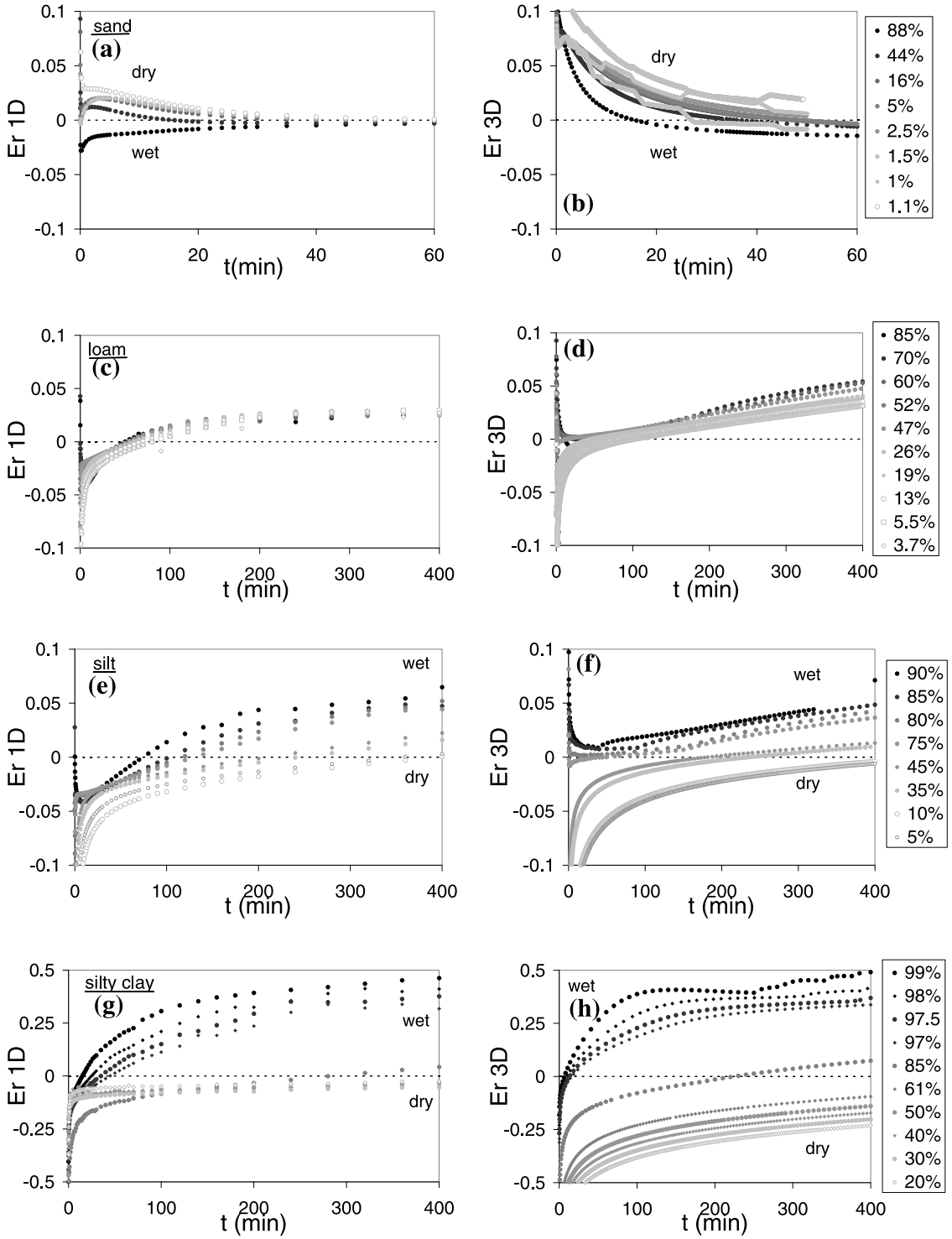

Figure 7. Accuracy of (a, c, e, g) $I_{3D}(t)$ and (b, d, f, h) $I_{1D}(t)$ defined using equations (1) and (3) with regard to numerically generated data. Initial saturations are shown on the right.

[1994] for describing 1-D and 3-D water cumulative infiltrations are studied in this paper. The 3-D case involves a specific case of water infiltrating from a surface disc source.

[52] A scaling procedure was proposed in the first part of the paper to derive equations describing one- and three-dimensional cumulative infiltrations and infiltration rates from the scaled cumulative infiltration and the scaled difference between 3-D and 1-D cumulative infiltrations. The analysis of analytical properties of scaled functions allows (1) complete demonstration of the analytical expressions of both scaled and dimensional direct approximations and (2) determination of related validity domains. In the second part of the paper, the focus was on the accuracy of

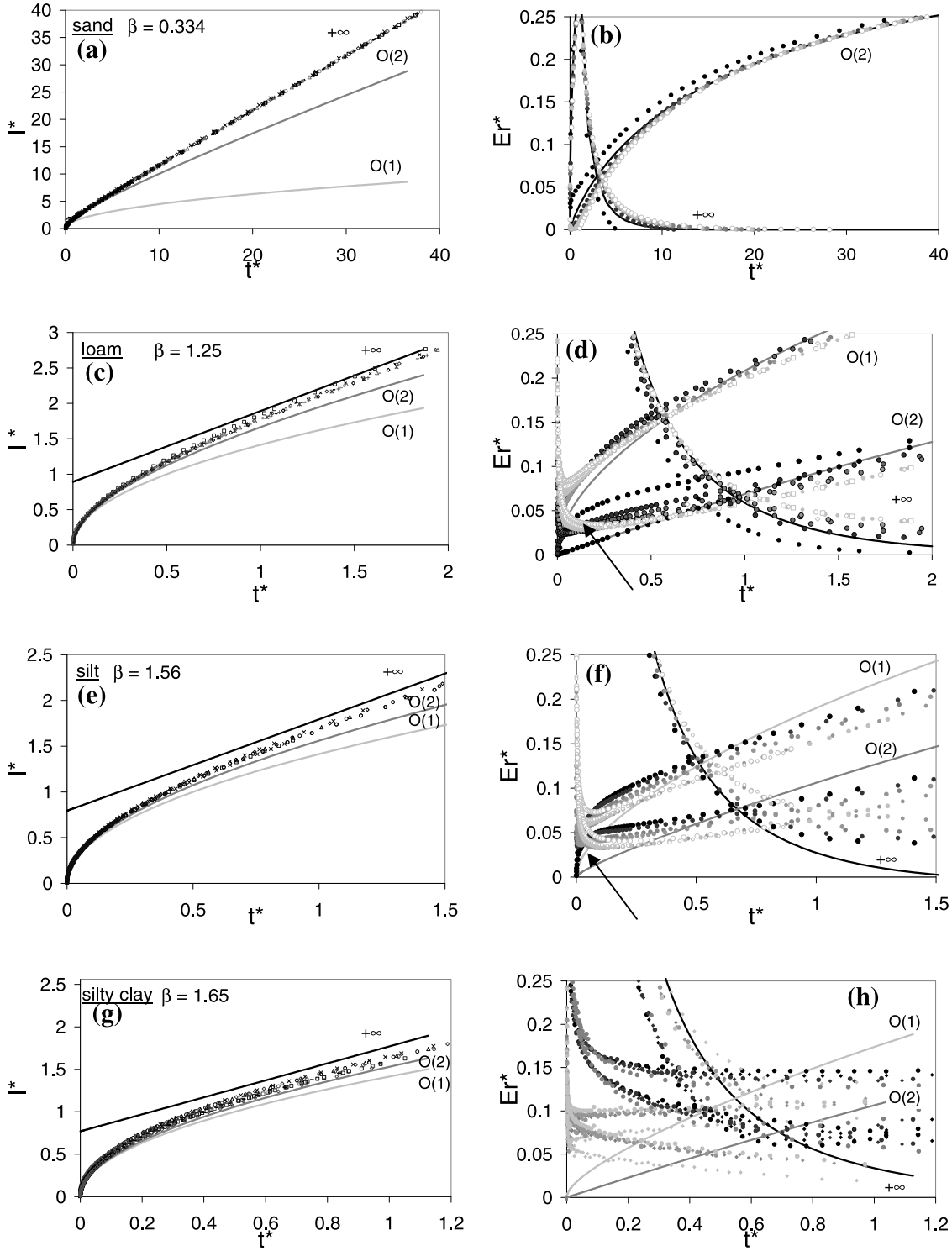

Figure 8. Scaled 1-D cumulative infiltrations $I^*_{num}(t^*)$ and first-order, second-order, and long-time approximations. (a, c, e, g) Numerical and analytical data and (b, d, f, h) relative errors between analytical and numerical curves (points) and between approximations and the quasi-exact formulation (lines). The arrows indicate the minimum second-order approximation model error.

the analytical models with respect to numerically generated one- and three-dimensional cumulative infiltrations for four soils (sand, loam, silt, and silty clay) and several initial saturations. The quasi-exact formulation was validated for sand, loam, and silt, provided that shape parameters γ and β, regarded as integral shape constants, are chosen as a function of the soil type. The proposed approximations derived for the same shape parameters and the proposed validity intervals were also validated for the same soils. Optimized values of the shape parameters β and γ were

quite different from the averaged values suggested by *Haverkamp et al.* [1994] (i.e., 0.75 and 0.6, respectively), but were close to those predicted by the Fuentes formulation [*Fuentes et al.*, 1992], especially for β. None of the analytical functions worked well for silty clay (a fine-textured soil), probably due to its unique hydraulic properties, which do not fulfill the conditions required for the validity of the quasi-exact formulation.

[53] This study proves that Haverkamp's formulations can be used to describe both 1-D and 3-D cumulative infiltrations, provided that great care is taken to determine the values of the corresponding shape parameters. Their values for three soil types from the ROSETTA database, i.e., sand, loam, and silt, are recommended. When the use of the quasi-exact formulation appears to be too complicated (due to its implicit formulation), direct approximations can be used, provided that these are restricted to the proposed validity intervals. Proposed values for validity times for sand, loam, and silt can be considered as good indicators for the choice between long-time, first-, or second-order approximations to analyze infiltration data.

[54] Further research is needed in several directions. First, the difference between 3-D and 1-D cumulative infiltrations in this study was only evaluated for one radius of the disc source, while *Warrick and Lazarovitch* [2007] and *Warrick et al.* [2007] have shown the dependency of the parameter γ upon the geometry of the infiltration source. The validity of the linear relationship for the difference between 3-D and 1-D cumulative infiltrations versus time, and the existence of the proportionality coefficient γ, needs to be confirmed for other radii of the disc source. Second, the dependence of the shape parameters β and γ on soil textural parameters should be established. Estimation of β using the approach used here for all textural classes of the ROSETTA database could confirm the hypothesis of an increase in β values for finer soils observed in this study. Third, there is a need to study constraints on soil hydraulic properties with regard to the conditions required by the quasi-exact formulation (equation (3)). This could help in defining the soils for which the quasi-exact formulation can be used, and those for which its use is not suitable. In particular, one should define the shape parameters of the analytical expressions of water retention and hydraulic conductivity functions, which fulfill conditions of the quasi-exact formulation. Additionally, correct values of β and γ need to be implemented into the BEST algorithm to avoid erroneous estimations of soil hydraulic characteristics.

Table 5. Dimensional Validity Times for Zero Initial Saturation and Errors of Approximations in Reproducing Dimensional 1-D and 3-D Numerical Cumulative Infiltrations

	$t_{Io(1)}$	$t_{Io(2)}$	$t_{I+\infty}$
Sand	<1″	2′30″	12′27″
Loam	2′32″	47′	3h15′
Silt	40′50″	3h′58″	19h22′
Silty clay	3h′	12h08′	2d14h
	1-D Maximum Model Errors		
Sand	NA	1.3%	3.4%
Loam	NA	4.8%	3.6%
Silt	8.7%	5.2%	5.7%
Silty clay	25.6%	18.4%	17.9%
	3-D Maximum Model Errors		
Sand	NA	7.6%	5.6%
Loam	NA	3.7%	2.40%
Silt	9.9%	4.9%	5.1%
Silty clay	17.3%	17.8%	21.8%

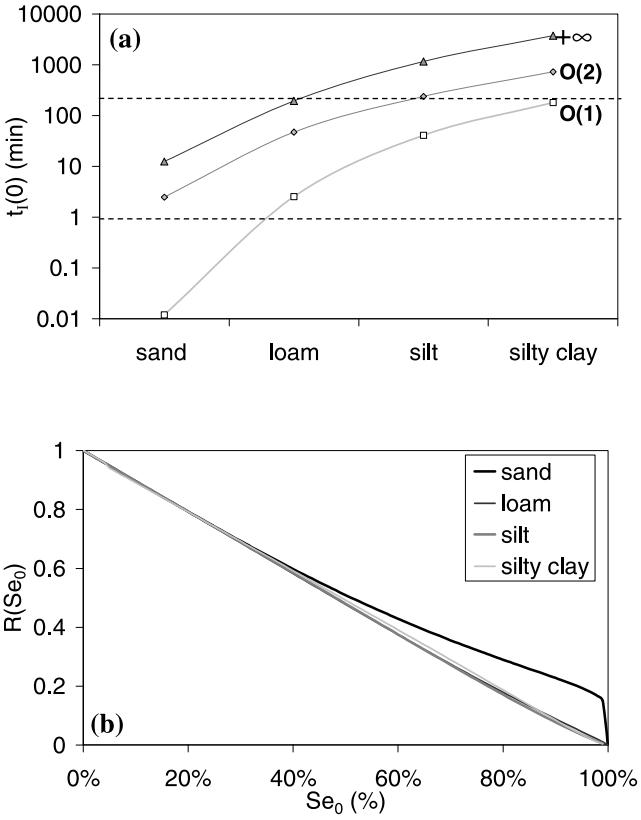

Figure 9. (a) Dimensional validity times for four types of soil and a zero initial saturation degree and time limits with regard to experimental constraints (horizontal lines) and (b) decrease of dimensional validity times versus the initial saturation Se_0.

Appendix A: Analysis of Scaled Cumulative Infiltration $I^*(t^*)$

[55] This appendix presents analytical properties of $I^*(t^*)$ and, in particular, its asymptotic behavior close to infinity or zero, when values of β are between zero and two. Let the function $I^*(t^*)$ be implicitly defined as follows:

$$t^* = \underbrace{\frac{1}{1-\beta}\left[I^* - \ln\left(\frac{\exp(\beta I^*)+\beta-1}{\beta}\right)\right]}_{RHS} \tag{A1}$$

[56] When t^* tends to infinity, I^* also tends to infinity. Using the properties of exponential and logarithmic functions, the following simplifications can be performed:

$$\ln\left(\frac{\exp(\beta I^*)+\beta-1}{\beta}\right) \approx \ln\left(\frac{\exp(\beta I^*)}{\beta}\right) = \beta I^* + \ln\left(\frac{1}{\beta}\right) \tag{A2}$$

Implementing (A2) into (A1) and resolving I^* as a function of t^* leads to the formulation of the long-time approximation:

$$I^*_{+\infty}(t) \approx t^* + \frac{1}{(1-\beta)} \ln\left(\frac{1}{\beta}\right) \tag{A3}$$

[57] Close to zero, $I^*(t^*)$ can be analyzed using a square-root-of-time series:

$$I^*(t^*) = \sum\nolimits_{k=1}^{+\infty} A_k t^{*k/2} \tag{A4}$$

considering only the first two terms of (A4), this corresponds to

$$I^*(t^*) = A_1 \sqrt{t^*} + A_2 t^* + \circ(t^*) \tag{A5}$$

where $\circ(t^{*n})$ represents neglected terms:

$$\circ(t^{*n}) = \sum_{k-n+1}^{+\infty} A_k t^{k/2} \tag{A6}$$

The right term of equation (A1), *RHS*, can be developed as a serial function when implementing the serial expansions of the exponential and logarithmic functions; then gathering exponent terms, we get

$$t^* = \frac{1}{2} A_1^2 t^* + A_1 \left(A_2 - \frac{A_1^2}{2}\left(\frac{2-\beta}{3}\right)\right) t^{3/2} + \circ\left(t^{3/2}\right) \tag{A7}$$

From equation (A7), we can obtain $A_1 = \sqrt{2}$ and $A_2 = \frac{2-\beta}{3}$. The expressions for the first- and second-order approximations can be written as

$$I^*_{\delta(1)}(t^*) = \sqrt{2t^*} \tag{A8a}$$

$$I^*_{\delta(2)}(t^*) = \sqrt{2t^*} + \frac{2-\beta}{3}\, t^* \tag{A8b}$$

Appendix B: Analysis of Scaled Infiltration Rate $q^*(t^*)$

[58] The scaled infiltration rate $q^*(t^*)$ can be obtained by evaluating the time derivative of both terms of the equation (A1), leading to

$$1 = \frac{1}{1-\beta}\left[q^* - q^* \frac{d}{dI^*} \ln\left(\frac{\exp(\beta I^*) + \beta - 1}{\beta}\right)\right] \tag{B1a}$$

which leads to

$$q^*(I^*) = 1 + \frac{\beta}{\exp(\beta I^*) - 1} \tag{B1b}$$

[59] From the property of the exponential function, it is clear that $q^*(I^*)$ tends toward unity for long times. Given a tolerance ξ, $q^*(I^*)$ for time t^* is as follows:

$$q^*(I^*(t^*)) \le 1 + \xi \tag{B2}$$

When using equation (B1b) and evaluating for I^* we get

$$\begin{gathered} I^* \ge I^*_{q+\infty} = \frac{1}{\beta} \ln\left(1 + \frac{\beta}{\xi}\right) \\ t^* \ge t^*_{q+\infty} \end{gathered} \tag{B3}$$

where $t^*_{q+\infty}$ is the time that corresponds to $I^*_{q+\infty}$. This can be derived from the equation (A1), leading to

$$t^*_{q+\infty}(\xi^*) = \frac{1}{(1-\beta)} \ln\left(\frac{\left(1 + \frac{\beta}{\xi^*}\right)^{\frac{1}{\beta}}}{1 + \frac{1}{\xi^*}}\right) \tag{B4}$$

This corresponds to equation (13) for the steady state validity time in the theory section.

[60] Close to zero time, the scaled cumulative infiltration $I^*(t^*)$ tends to zero. Hence, the scaled infiltration flux $q^*(t^*)$ tends to infinity (equation (B1b)). Short time approximations of $q^*(I^*)$ can be defined using the series expansions of $\exp(x)$ and $(1 + x)^{-1}$ leading to

$$q^*_{\delta(1)}(I^*) = \frac{1}{I^*} \tag{B5a}$$

$$q^*_{\delta(2)}(I^*) = \frac{1}{I^*} + 1 - \frac{\beta}{2} \tag{B5b}$$

These approximations can be combined with the short-time expansions of $I^*(t^*)$ to give

$$q^*_{\delta(1)}(t^*) = \frac{1}{\sqrt{2}} t^{*-\frac{1}{2}} \tag{B6a}$$

$$q^*_{\delta(2)}(t^*) = \frac{1}{\sqrt{2}} t^{*-\frac{1}{2}} + \frac{2-\beta}{3} \tag{B6b}$$

[61] These expressions correspond to equations (14) and (15) in the theory section. Note that these approximations, such as $q^*(t^*)$, are not defined at time zero (they converge to infinity when time approaches zero). Also note that the proposed approach to determine the expressions for $q^*_{\delta(1)}(t^*)$ and $q^*_{\delta(2)}(t^*)$ using the serial expansions is a more proper way than directly calculating derivatives from the analytical expressions for $I^*_{\delta(1)}(t^*)$ and $I^*_{\delta(2)}(t^*)$ (equations (A8a) and (A8b)). Actually, derivating term by term a serial function does not always lead to a proper definition of its derivate. To do so, the series require specific analytical properties [*Ayres and Mendelson*, 1999].

References

Angulo-Jaramillo, R., J. P. Vandervaere, S. Roulier, J. L. Thony, J. P. Gaudet, and M. Vauclin (2000), Field measurement of soil surface

hydraulic properties by disc and ring infiltrometers: A review and recent developments, *Soil Tillage Res.*, *55*, 1–29, doi:10.1016/S0167-1987(00)00098-2.

Ayres, F., Jr., and E. Mendelson (1999), *Schaum's Outline of Calculus*, McGraw-Hill, New York.

Basha, H. A. (1999), Multidimensional linearized nonsteady infiltration with prescribed boundary conditions at the soil surface, *Water Resour. Res.*, *35*, 75–93, doi:10.1029/1998WR900015.

Basha, H. A. (2002), Burger's equation: A general nonlinear solution of infiltration and redistribution, *Water Resour. Res.*, *38*(11), 1247, doi:10.1029/2001WR000954.

Braester, C. (1973), Moisture variation at the soil surface and the advance of the wetting front during infiltration at constant flux, *Water Resour. Res.*, *9*, 687–694, doi:10.1029/WR009i003p00687.

Braud, I., R. Haverkamp, J. L. Arrúe, and M. V. López (2003), Spatial variability of soil surface properties and consequences for the annual and monthly water balance of a semiarid environment (EFEDA experiment), *J. Hydrometeorol.*, *4*, 121–137, doi:10.1175/1525-7541(2003)004<0121:SVOSSP>2.0.CO;2.

Braud, I., D. De Condappa, J. M. Soria, R. Haverkamp, R. Angulo-Jaramillo, S. Galle, and M. Vauclin (2005), Use of scaled forms of the infiltration equation for the estimation of unsaturated soil hydraulic properties (*Beerkan* method), *Eur. J. Soil Sci.*, *56*, 361–374, doi:10.1111/j.1365-2389.2004.00660.x.

Campbell, S., J. P. Chancelier, and R. Nikoukhah (2006), *Modeling and Simulation in Scilab/Scicos*, Springer, New York.

Clausnitzer, V., J. W. Hopmans, and J. L. Starr (1998), Parameter uncertainty analysis of common infiltration models, *Soil Sci. Soc. Am. J.*, *62*, 1477–1487.

Feddes, R. A., P. Kabat, P. J. T. Vanbakel, J. J. B. Bronswijk, and J. Halbertsma (1988), Modelling soil water dynamics in the saturated zone—State of the art, *J. Hydrol.*, *100*, 69–111, doi:10.1016/0022-1694(88)90182-5.

Fuentes, C., R. Haverkamp, and J. Y. Parlange (1992), Parameter constraints on closed-form soil water relationships, *J. Hydrol.*, *134*, 117–142, doi:10.1016/0022-1694(92)90032-Q.

Galle, S., et al. (2001), Estimation of soil hydrodynamic properties of the Donga watershed (CATCH-Bénin), paper presented at GEWEX 4th International Conference, Global Energy and Water Cycle Exp., Paris, 10–14 Sept.

Green, W. H., and G. Ampt (1911), Studies on soil physics, 1. The flow of air and water through soils, *J. Agric. Sci.*, *4*(1), 1–24, doi:10.1017/S0021859600001441.

Haverkamp, R., J. Y. Parlange, J. L. Starr, G. Schmitz, and C. Fuentes (1990), Infiltration under ponded conditions: 3. A predictive equation based on physical parameters, *Soil Sci.*, *149*, 292–300, doi:10.1097/00010694-199005000-00006.

Haverkamp, R., P. J. Ross, K. R. J. Smetten, and J. Y. Parlange (1994), Three-dimensional analysis of infiltration from the disc infiltrometer: 2. Physically based infiltration equation, *Water Resour. Res.*, *30*, 2931–2935, doi:10.1029/94WR01788.

Haverkamp, R., J. L. Arrúe, J. P. Vandervaere, I. Braud, G. Boulet, J. P. Laurent, A. Taha, P. J. Ross, and R. Angulo-Jaramillo (1996), Hydrological and thermal behaviour of the vadose zone in the area of Barrax and Tomelloso (Spain): Experimental study, analysis and modeling, *Proj. UE EV5C-CT 92 00 90*, Eur. Union, Brussels.

Haverkamp, R., F. Bouraoui, C. Zammit, R. Angulo-Jaramillo, and J. W. Delleur (1999), Soil properties and moisture movement in the unsaturated zone. 2931–2935, in *The Handbook of Groundwater Engineering*, edited by J. W. Delleur, pp. 5.1–5.50, CRC Press, Boca Raton, Fla.

Haverkamp, R., D. Debionne, P. Viallet, R. Angulo-Jaramillo, and D. de Condapa (2005), Soil properties and moisture movement in the unsaturated zone, in *The Handbook of Groundwater Engineering*, edited by J. W. Delleur, pp. 1–59, CRC Press, Boca Raton, Fla.

Jacques, D., B. P. Mohanty, and J. Feyen (2002), Comparison of alternative methods for deriving hydraulic properties and scaling factors from single-disc tension infiltrometer measurements, *Water Resour. Res.*, *38*(7), 1120, doi:10.1029/2001WR000595.

Lassabatere, L., R. Angulo-Jaramillo, J. M. Soria Ugalde, R. Cuenca, I. Braud, and R. Haverkamp (2006), Beerkan estimation of soil transfer parameters through infiltration experiments—BEST, *Soil Sci. Soc. Am. J.*, *70*, 521–532, doi:10.2136/sssaj2005.0026.

Lin, H. S., and K. J. McInnes (1995), Water flow in clay soil beneath a tension infiltrometer, *Soil Sci.*, *159*, 375–382, doi:10.1097/00010694-199506000-00002.

Mallants, D., D. Jacques, P. H. Tseng, M. T. van Genuchten, and J. Feyen (1997), Comparison of three hydraulic property measurement methods, *J. Hydrol.*, *199*, 295–318, doi:10.1016/S0022-1694(96)03331-8.

Messing, I., and N. J. Jarvis (1993), Temporal variation in the hydraulic conductivity of a tilled clay soil as measured by tension infiltrometers, *J. Soil Sci.*, *44*, 11–24, doi:10.1111/j.1365-2389.1993.tb00430.x.

Mualem, Y. (1976), A new model for predicting the hydraulic conductivity of unsaturated porous media, *Water Resour. Res.*, *12*, 513–522, doi:10.1029/WR012i003p00513.

Parlange, J.-Y. (1975), On solving the flow equation in unsaturated soil by optimization: Horizontal infiltration, *Soil Sci. Soc. Am. J.*, *39*, 415–418.

Parlange, J.-Y., I. Lisle, R. D. Braddock, and R. E. Smith (1982), The three parameter infiltration equation, *Soil Sci.*, *133*, 337–341, doi:10.1097/00010694-198206000-00001.

Parlange, J.-Y., R. Haverkamp, and J. Touma (1985), Infiltration under ponded conditions: 1. Optimal analytical solution and comparison with experimental observations, *Soil Sci.*, *139*, 305–311.

Perroux, K. M., and I. White (1988), Designs for disc permeameters, *Soil Sci. Soc. Am. J.*, *52*, 1205–1215.

Philip, J. R. (1969), Theory of infiltration, *Adv. Hydrosci.*, *5*, 215–296.

Philip, J. R. (1973), On solving the unsaturated flow equation: 1. The flux-concentration relation, *Soil Sci.*, *116*, 328–335, doi:10.1097/00010694-197311000-00002.

Rasoulzadeh, A., and A. R. Sepaskhah (2003), Scaled infiltration equations for furrow irrigation, *Biosyst.Eng.*, *86*, 375–383, doi:10.1016/j.biosystemseng.2003.07.004.

Ross, P. J., R. Haverkamp, and J.-Y. Parlange (1996), Calculating parameters for infiltration equation from soil hydraulic functions, *Transp. Porous Media*, *24*, 315–339, doi:10.1007/BF00154096.

Salvucci, G., and D. Entekhabi (1994), Explicit expressions for Green-Ampt (delta function diffusivity) infiltration rate and cumulative storage, *Water Resour. Res.*, *30*, 2661–2663, doi:10.1029/94WR01494.

Schaap, M. G., F. J. Leij, and M. T. van Genuchten (2001), ROSETTA: A computer program for estimating soil hydraulic parameters with hierarchical pedotransfer functions, *J. Hydrol.*, *251*, 163–176, doi:10.1016/S0022-1694(01)00466-8.

Šimůnek, J., and M. T. van Genuchten (1996), Estimating unsaturated soil hydraulic properties from tension disc infiltrometer data by numerical inversion, *Water Resour. Res.*, *32*, 2683–2696, doi:10.1029/96WR01525.

Šimůnek, J., and M. T. van Genuchten (2008), Modeling nonequilibrium flow and transport processes using HYDRUS, *Vadose Zone J.*, *7*, 782–797, doi:10.2136/vzj2007.0074.

Šimůnek, J., R. Angulo-Jaramillo, M. G. Schaap, J. P. Vandervaere, and M. T. van Genuchten (1998), Using an inverse method to estimate the hydraulic properties of crusted soils from tension-disc infiltrometer data, *Geoderma*, *86*, 61–81, doi:10.1016/S0016-7061(98)00035-4.

Šimůnek, J., M. T. van Genuchten, and M. Šejna (2006), The HYDRUS software package for simulating two- and three-dimensional movement of water, heat, and multiple solutes in variably saturated media, version 1.0, technical manual, PC Progress, Prague.

Šimůnek, J., M. Šejna, H. Saito, M. Sakai, and M. T. van Genuchten (2008), The HYDRUS-1D software package for simulating the one-dimensional movement of water, heat, and multiple solutes in variably saturated media, version 4.0, *HYDRUS Software Ser. 3*, Dep. of Environ. Sci., Univ. of Calif., Riverside.

Smetten, K. R. J., J. Y. Parlange, P. J. Ross, and R. Haverkamp (1994), Three-dimensional analysis of infiltration from the disc infiltrometer: 1. A capillary-base theory, *Water Resour. Res.*, *30*, 2925–2929.

Smith, R. E., K. R. J. Smetten, P. Broadbridge, and D. A. Woolhiser (2002), *Infiltration Theory for Hydrology Applications*, *Geophys. Monogr. Ser.*, vol. 129, AGU, Washington.

Turner, N. C., and J. Y. Parlange (1974), Lateral movement at the periphery of a one-dimensional flow of water, *Soil Sci.*, *118*(2), 70–77, doi:10.1097/00010694-197408000-00002.

Vandervaere, J. P., M. Vauclin, and D. E. Elrick (2000a), Transient flow from tension infiltrometers: II. Four methods to determine sorptivity and conductivity, *Soil Sci. Soc. Am. J.*, *64*, 1272–1284.

Vandervaere, J. P., M. Vauclin, and D. E. Elrick (2000b), Transient flow from tension infiltrometers: I. The two-parameter equation, *Soil Sci. Soc. Am. J.*, *64*, 1263–1272.

van Genuchten, M. T. (1980), A closed form equation for predicting the hydraulic conductivity of unsaturated soils, *Soil Sci. Soc. Am. J.*, *44*, 892–898.

Varado, N., I. Braud, P. J. Ross, and R. Haverkamp (2006), Assessment of an efficient numerical solution of the 1D Richards' equation on bare soil, *J. Hydrol.*, *323*, 244–257, doi:10.1016/j.jhydrol.2005.07.052.

Warrick, A. W., and N. Lazarovitch (2007), Infiltration from a strip source, *Water Resour. Res.*, *43*, W03420, doi:10.1029/2006WR004975.

Warrick, A. W., N. Lazarovitch, A. Furman, and D. Zerihun (2007), Explicit infiltration function for furrows, *J. Irrig. Drain.*, *133*(4), 307–313, doi:10.1061/(ASCE)0733-9437(2007)133:4(307).

Zhu, J., and B. P. Mohanty (2002), Analytical solutions for steady-state vertical infiltration, *Water Resour. Res.*, *38*(8), 1145, doi:10.1029/2001WR000398.

R. Angulo-Jaramillo, Laboratoire des Sciences de l'Environnement, Ecole Nationale des Travaux Publics de l'Etat, Rue Maurice Audin, F-69518 Vaulx-en-Velin, France.

R. Haverkamp, Laboratoire d'Etude des Transferts en Hydrologie et Environnement, CNRS, F-38041 Grenoble, France.

L. Lassabatere, Division Eau et Environnement, LCPC, Route de Bouaye, F-44341 Bouguenais, France. (laurent.lassabatere@lcpc.fr)

J. Šimůnek, Department of Environmental Sciences, University of California, Riverside, CA 92521, USA.

J. M. Soria-Ugalde, Departamento de Ingeniería Geomática e Hidráulica, Universidad de Guanajuato, Avenida Juárez 77, 36000 Guanajuato, Mexico.